1992A&A...265..328B

Astron. Astrophys. 265, 328–344 (1992)

ASTRONOMY
AND
ASTROPHYSICS

Stratification and thermodynamics in mean-field dynamos

Axel Brandenburg[1,2], **David Moss**[3], **and Ilkka Tuominen**[2]

[1] NORDITA, Blegdamsvej 17, DK-2100 Copenhagen Ø, Denmark
[2] Observatory and Astrophysics Laboratory, University of Helsinki, Tähtitorninmäki, SF-00130 Helsinki, Finland
[3] Mathematics Department, The University, Manchester M13 9PL, UK

Received February 28, accepted July 12, 1992

Abstract. We extend previous investigations of axisymmetric, incompressible mean-field dynamos to the compressible case with strong stratification. We take thermodynamic effects into account using the anelastic approximation and show that the effects of stratification, compressibility and thermodynamics on the rotation law are small when we compare our results with those previously obtained for incompressible models. For solar values of the Taylor number cylindrical contours of the angular velocity typically occur – even for strong stratification. The stagnation line of the meridional circulation is close to the bottom of the convection zone. In the presence of magnetic fields the meridional flow is amplified, in particular close to the surface where the density is small and the Lorentz force per unit mass, $\boldsymbol{J} \times \boldsymbol{B}/\rho$, is large. The depth dependence of the magnetic energy density, however, is not much altered by the inclusion of a density stratification. For cyclical dynamo magnetic fields thermal and magnetic energies are approximately in antiphase. The cyclic variation in luminosity is small and it lags the variation in magnetic energy by approximately 1/8 of the period. For $\alpha\partial\Omega/\partial r > 0$ we find poleward migrating dynamo waves, whilst for $\alpha\partial\Omega/\partial r < 0$ our solutions are steady or oscillatory, depending on the boundary condition for the magnetic field at the bottom of the convection zone.

Key words: The Sun: magnetic fields – stars: magnetic fields – hydromagnetics – turbulence – convection

1. Introduction

A number of nonlinear $\alpha\Omega$-dynamo models have been investigated in the past (e.g. Rüdiger 1973; Jepps 1975; Ivanova & Ruzmaikin 1977; Brandenburg et al. 1989; Schmitt & Schüssler 1989; Jennings 1991). One goal of this type of work is to understand the solar 22-year magnetic activity cycle. In these models the angular velocity Ω is not obtained simultaneously as a solution of the momentum equations, but is considered as given. It is then possible to construct models whose magnetic field geometry closely resembles the observed one. Although considerable insight into dynamo mechanisms has been obtained from these models, the approach is necessarily dynamically inconsistent and so unsatisfactory.

Send offprint requests to: A. Brandenburg, NORDITA

In a series of papers Gilman and Glatzmaier investigated dynamo action from convection in spherical shells, seeking self-consistent models for the solar cycle (e.g. Gilman & Miller 1981; Gilman 1983; Glatzmaier 1985). Their main result is that the equatorial angular velocity decreases outwards and that magnetic cycles occur for sufficiently small magnetic diffusivity, accompanied by a *poleward* migration of magnetic fields. The unresolved small scale behaviour is taken into account only by the use of enhanced diffusivities, ie there is no parametrization of anisotropies in the small scale motions.

An intermediate approach is to aim for a more consistent solution of the $\alpha\Omega$-type mean-field dynamo. In previous papers (Brandenburg et al. 1990a, 1991a, 1992; hereafter referred to as Papers I, II, III, respectively) we investigated mean-field dynamos, in which generation of differential rotation by Reynolds stresses is parametrized by the Λ-effect (Rüdiger 1980, 1989) and where the feedbacks between the magnetic field and the flow are included. In these models we assumed the density to be uniform and constant. We found oscillatory dynamo solutions with field migration only when the turbulent magnetic diffusivity η_t is small enough. On the other hand, from investigations of incompressible models it appears that the turbulent kinematic viscosity ν_t must not be too small, because otherwise cylindrical Ω-contours occur (Köhler 1970), contradicting helioseismological observations (Brown & Morrow 1986). On theoretical grounds it is hard to accept large values for the turbulent magnetic Prandtl number $\mathrm{Pr}_M = \nu_t/\eta_t$. Thus, some essential ingredients of the solar dynamo appear still to be missing from that theory.

Various possibilities have been previously discussed which may cause deviations from a rotation law that has Ω constant on cylinders. These include, for example, higher order terms in the expansion for the Λ-effect (Rüdiger 1989), and the effects of compressibility and stratification. Stix (1989) pointed out that a sufficiently large latitudinal entropy gradient is likely to relax the conditions under which the Taylor-Proudman theorem applies. In particular, models with generation of differential rotation by a latitudinal dependent heat transport have been presented which do not display cylindrical Ω-contours even for high Taylor numbers; see Fig. 4 in Schmidt (1982). However, it is not clear to what extent the adopted linearization is valid for high Taylor numbers.

The purpose of the present paper is to investigate the effects of stratification and thermodynamics in dynamos, adopting the framework of mean-field theory. We thus consider the large scale behaviour of velocity, magnetic and temperature fields whilst the

© European Southern Observatory • Provided by the NASA Astrophysics Data System

1992A&A...265..328B

small scale behaviour of the flow is parametrized by various turbulent transport coefficients. Systematic azimuthal variations of the large scale flow in the Sun are probably of secondary importance and so we restrict ourselves here to axisymmetric mean fields. We choose constant profiles for various coefficients throughout the convection zone. The radiative interior is excluded from the computational domain by assuming suitable boundary conditions. Preliminary results have been reported in Brandenburg et al. (1991b). Here we are merely interested in the gross effects of stratification. It appears too early to attempt a detailed tuning of the model to solar conditions at this stage. In particular, the complex physical situation at the bottom of the convection zone may introduce new complications that have to be studied separately (cf. Paper III).

This paper is organized as follows. In Sect. 2 we present the basic equations and boundary conditions. In Sect. 3 we reformulate these equations in a numerically convenient form. Test calculations for our compressible code are presented in Sect. 4. In Sect. 5 we give the results for different cases and, finally, in Sect. 6 we discuss the uncertainties inherent in our approach and in Sect. 7 we present our conclusions.

2. Basic equations

We consider the initial value problem of a conducting fluid in a rotating spherical shell with inner and outer radii r_0 and R. We solve the hydromagnetic mean-field equations, starting with a rigid rotation with angular velocity, Ω_0, and a weak magnetic seed-field. We are interested in the evolution of velocity and magnetic fields on time scales that are much longer than the sound travel time. We can therefore adopt the anelastic approximation (e.g. Gough 1969).

2.1. The hydromagnetic mean-field equations

The equations governing the generation of mean magnetic field by an α-effect and differential rotation by Reynolds stresses, $\mathcal{Q}$, are

$$\frac{\partial \boldsymbol{B}}{\partial t} = \mathrm{curl}\,(\boldsymbol{u}\times\boldsymbol{B} + \alpha\boldsymbol{B} - \eta_t\mu_0\boldsymbol{J}), \tag{1}$$

$$\rho\frac{\mathrm{D}\boldsymbol{u}}{\mathrm{D}t} = -\nabla p + \rho\boldsymbol{g} + \boldsymbol{J}\times\boldsymbol{B} - \mathrm{Div}\,(\rho\mathcal{Q} - \mathcal{B}), \tag{2}$$

$$\rho T\frac{\mathrm{D}s}{\mathrm{D}t} = -\mathrm{div}\,\boldsymbol{F} + q, \tag{3}$$

with

$$\mathrm{div}\,\rho\boldsymbol{u} = \mathrm{div}\,\boldsymbol{B} = 0. \tag{4}$$

Here, $\mathrm{D}/\mathrm{D}t = \partial/\partial t + \boldsymbol{u}\cdot\nabla$ denotes the total derivative, $\boldsymbol{g}$ gravity, $\boldsymbol{J} = \mathrm{curl}\,\boldsymbol{B}/\mu_0$ the electric current, μ_0 the induction constant, η_t the magnetic diffusivity, $\mathcal{Q}_{ij} = \langle u_i'u_j'\rangle$ the Reynolds stress tensor, and $\mathcal{B}_{ij} = \langle B_i'B_j'\rangle - \frac{1}{2}\delta_{ij}\langle \boldsymbol{B}'^2\rangle$ the Maxwell stress tensor. We make the common assumption of neglecting correlations between velocity and density fluctuations. For $\mathcal{Q}$ we adopt the form

$$\mathcal{Q}_{ij} = \mathcal{Q}_{ij}^{(\Lambda)} - \nu_t(u_{i,j} + u_{j,i}) - \mu_t\delta_{ij}\mathrm{div}\,\boldsymbol{u} \tag{5}$$

(Rüdiger 1980), where ν_t and μ_t are turbulent viscosities, and i, j refer here to Cartesian coordinates. The last two terms on the right hand side of Eq. (5) describe a diffusive transport of angular momentum. The first term is the Λ-effect with $\mathcal{Q}_{ij}^{(\Lambda)} = (\hat{\phi}_j\Lambda_i + \hat{\phi}_i\Lambda_j)\Omega$, where $i, j = r, \theta, \phi$ are spherical polar coordinates, $\hat{\boldsymbol{\phi}}$ is the unit vector in the ϕ-direction, $\boldsymbol{\Omega} = \hat{\boldsymbol{z}}u_\phi/\varpi$ is the rotation vector, $\hat{\boldsymbol{z}}$ is the unit vector along the axis of rotation, $\varpi = r\sin\theta$ is the distance from the rotation axis, and $\boldsymbol{\Lambda} = (\Lambda_V\sin\theta, \Lambda_H\cos\theta, 0)$, or explicitly in spherical polar coordinates

$$\mathcal{Q}^{(\Lambda)} = \begin{pmatrix} 0 & 0 & \Lambda_V\sin\theta \\ 0 & 0 & \Lambda_H\cos\theta \\ \Lambda_V\sin\theta & \Lambda_H\cos\theta & 0 \end{pmatrix}\Omega. \tag{6}$$

Following Rüdiger (1980) we represent Λ by

$$\Lambda_\mathrm{V} = \nu_t(V^{(0)} + V^{(1)}\sin^2\theta),\quad \Lambda_\mathrm{H} = \nu_t H^{(1)}\sin^2\theta, \tag{7}$$

where $V^{(0)}$, $V^{(1)}$ and $H^{(1)}$ are expected to be of order of unity. There are also nondiffusive contributions to $\mathcal{Q}_{r\theta}$ which certainly do not vanish. We neglect them here because hardly anything is known about their sign and magnitude. This term does not appear in the toroidal part of the momentum equation and therefore is not directly important for the rotation law. However, $\mathcal{Q}_{r\theta}$ may be important for modifying meridional flows, and may so indirectly influence the rotation law. We also neglect the tensor $\mathcal{B}$ because of the uncertainties associated with it. Note that Roberts & Soward (1975) found for this tensor

$$\mathcal{B}_{ij} = -\eta_t/\eta\,(B_iB_j + \tfrac{1}{2}\delta_{ij}\boldsymbol{B}^2), \tag{8}$$

where η is the laminar magnetic diffusivity. For $\eta_t > \eta$ the minus sign in Eq. (8) could modify strongly any saturation of the dynamo by the action of the Lorentz force on the mean flow. If the efficiency of this mechanism were to be markedly reduced then, in the context of our models, saturation would have to arise from α- and Λ-quenching mechanisms (Rüdiger & Kichatinov 1990). Equation (8) was derived using the first order smoothing approximation which may be questionable for large values of η_t/η (Rüdiger et al. 1986). In the Sun, where magnetically induced flows (e.g. torsional oscillations) can perhaps be considered as a small perturbations, we might anyway expect that the tensor $\mathcal{B}$ is less important than $\mathcal{Q}$. Clearly, effects arising from the tensor $\mathcal{B}$ deserve a separate investigation. In the present work we consider primarily the magnetic feedback on the mean motions arising from the large scale magnetic field.

2.2. The convective flux

In the bulk of the convection zone the radiative flux is small compared with the convective flux of the (turbulent) small scale motions, so we assume $\boldsymbol{F} = \boldsymbol{F}^{\mathrm{conv}}$, where $\boldsymbol{F}^{\mathrm{conv}} \approx \rho c_p\langle \boldsymbol{u}'T'\rangle$. Close to the bottom of the convection zone the radiative flux becomes important compared with the convective flux, but it is nevertheless irrelevant directly for the dynamics, because the radiative time scale is much longer than the solar cycle period. This assumption is of similar nature as the approximation that the diffusivity, as well as the α and Λ coefficients, are taken as constant and non-vanishing at the boundaries. (But the implied reduction in turbulent transport coefficients may nevertheless be important.) The interior or interactions with it are excluded by our choice of boundary conditions. Effects arising from the complex and ill-understood interface between the convection zone and the radiative interior are here ignored and postponed to a further investigation (preliminary results are reported in Paper III). Thus our model only describes the region within the formal convection zone.

In the simplest approximation the convective flux is proportional to the entropy gradient with

© European Southern Observatory • Provided by the NASA Astrophysics Data System

1992A&A...265..328B

$$\boldsymbol{F}^{\text{conv}} = -\chi_t \rho T \nabla s, \tag{9}$$

(e.g. Durney & Roxburgh 1971), where χ_t is the turbulent heat conductivity. We specify the ratios between the various diffusivities by the Prandtl number $\Pr = \nu_t/\chi_t$, the magnetic Prandtl number $\Pr_M = \nu_t/\eta_t$, and $P_\mu = \mu_t/\nu_t$.

The temperature T and the density ρ are functions of pressure p and specific entropy s. We assume a perfect gas with

$$\rho T = \frac{p}{c_p \nabla_{\text{ad}}}, \quad \ln \rho = \frac{1}{\gamma} \ln p - \frac{1}{c_p} s, \quad \ln T = \nabla_{\text{ad}} \ln p + s/c_p, \tag{10}$$

where $\nabla_{\text{ad}} = 1 - 1/\gamma$ and γ is the ratio of the specific heats c_p and c_v, which we assume to be constant. In the following we take $\gamma = 5/3$, ie $\nabla_{\text{ad}} = 0.4$. We neglect heat sources (such as viscous and Joule heating) and so put $q = 0$ in Eq. (3). Furthermore, we assume that the mass $M_c = \int_V \rho dV$ contained in the convection zone with volume V is negligible compared to the mass of the star, M, and so neglect self-gravitational effects. The (invariant) gravitational acceleration is then given by $\boldsymbol{g} = -\hat{\boldsymbol{r}} g$, where $g = GM/r^2$.

2.3. Boundary and initial conditions

We assume the bottom of the convection zone ($r = r_0$) to be an impenetrable, stress free, electrically perfect conductor with a constant energy flux corresponding to the luminosity $L = 4\pi r_0^2 F(r_0)$ of the star. The upper surface is assumed to be a stress free blackbody radiator ($F = \sigma T^4$), from which magnetic fields continue into the outer space as potential fields. As an alternative to the blackbody assumption, we can fit to the radiative zero solution. Using Kramers' opacity law, the relation between pressure and temperature is given then by $p^2 = KT^{8.5}$ with $K = \frac{2}{8.5} \frac{4ac}{3} \frac{k}{H} \frac{4\pi GM}{\mu \kappa_0 L}$ (see Schwarzschild 1958, §11). Here we can replace L by $4\pi R^2 F$ and interpret F as the latitudinal dependent flux. Thus we can then take as outer boundary condition

$$F \propto p^a T^b \tag{11}$$

with $a = -2$ and $b = 8.5$. The blackbody radiator condition ($F \propto T^4$) is recovered by taking $a = 0$ and $b = 4$. As a further possibility we may adopt a fit to a convective upper layer, which implies $a = -0.4$ and $b = 1$.

The initial and reference state is assumed to be a solution of Eqs. (2) and (3) for $\boldsymbol{u} = \boldsymbol{B} = 0$, which give

$$r^2 \rho_0^{-1} dp_0/dr = -GM = \text{const}, \tag{12}$$

$$r^2 p_0 \, ds_0/dr = -c_p \nabla_{\text{ad}} L/(4\pi\chi_t) = \text{const}. \tag{13}$$

2.4. Nondimensional control parameters

As nondimensional measures for gravity and luminosity we use

$$\Gamma = GMR/\nu_t^2, \tag{14}$$

$$\mathscr{L} = \nabla_{\text{ad}} LR/(4\pi\overline{\rho}\nu_t^3), \tag{15}$$

where $\overline{\rho} = M_c/V$ is the mean density in the convection zone. Note that M_c is constant for impenetrable upper and lower boundaries.

The strength of the stratification is controlled by the surface value of the ratio $\xi = H_p/R$, where $H_p = p_0/(\rho_0 g) = \nabla_{\text{ad}} c_p T_0/g$ is the pressure scale height, ie

$$\xi = \nabla_{\text{ad}} c_p T_S R/(GM), \tag{16}$$

where $T_S = T_0(R)$ is the outer temperature of the reference solution of Eq. (12) and (13). The strength of stratification can also be measured in terms of the number of pressure scale heights $N_p = \ln(p_{\text{bot}}/p_{\text{top}})$ or, equivalently, the number of density scale heights included; $N_\rho = \ln(\rho_{\text{bot}}/\rho_{\text{top}})$. For the special case of an adiabatic reference solution we have

$$N_p = \nabla_{\text{ad}}^{-1} \ln[1 + \xi^{-1}\nabla_{\text{ad}}(R/r_0 - 1)]. \tag{17}$$

Below, we adopt $\xi = 0.01$ which corresponds to $N_p = 7.2$, and $N_\rho = 4.3$.

A "turbulent" Rayleigh number may be defined as

$$\text{Ra} = \left(-\frac{gd^4}{\chi_t \nu_t} \frac{1}{c_p} \frac{ds_0}{dr} \right)_{r=r_m} = \Pr^2 \mathscr{L} \left(\frac{d}{r_m} \right)^4 \frac{GM\overline{\rho}}{Rp_m}, \tag{18}$$

where $r_m = \frac{1}{2}(r_0 + R)$ is the mean radius of the shell, and $p_m = p_0(r_m)$. This definition of Ra agrees with that of Glatzmaier & Gilman (1981).

Equations (12) and (13) can be integrated between r_0 and R for given M_c and M once ξ, Γ, $\mathscr{L}$, are specified. Having obtained a hydrostatic equilibrium configuration, we introduce a velocity field corresponding to a uniform rotation with angular velocity Ω_0. The corresponding nondimensional parameter is the Taylor number,

$$\text{Ta} = 4\Omega_0^2 R^4/\nu_t^2. \tag{19}$$

We choose to work in an inertial frame of reference, because the variations in the angular velocity, produced by the Λ-effect, are found to be of the order of the angular velocity itself. In the presence of rotation the hydrostatic reference solution of Eqs. (12) and (13) no longer satisfies Eq. (2), and so the system will approach a state where ρ and p also depend on latitude. In the adiabatic case ($\mathscr{L} = 0$) without Λ-effect, an initially nonuniform rotation leads after some time to uniform rotation with $\Omega = \Omega_0$.

The strength of the α-effect is measured by

$$C_\alpha = \alpha_0 R/\eta_t, \tag{20}$$

where α_0 is a characteristic value for α. Here, we assume $\alpha = \alpha_0 \cos\theta$. In two cases we also include the effect of α-quenching using $\alpha = \alpha_0 \cos\theta/(1+\alpha_B \boldsymbol{B}^2)$. Simple estimates suggest that $C_\alpha \approx \frac{1}{2}\Pr_M \text{Ta}^{1/2}\xi_{\text{cor}}$ and $\alpha_B = \frac{1}{9}\xi_{\text{cor}}^2$, where $\xi_{\text{cor}} = \ell_{\text{cor}}/R$ is the normalized correlation length (see Paper I).

2.5. Solar values

In order to get some feeling for the parameters introduced above we can insert solar values: $R_\odot = 7\,10^{10}$ cm, $L_\odot = 3.9\,10^{33}$ g cm^2/s^3, $GM_\odot = 1.34\,10^{26}$ cm^3/s^2, $M_c = 6\,10^{31}$g, $\Omega_0 = 3\,10^{-6}$ s^{-1}, $\nu_t = \eta_t = 5\,10^{12}$ cm^2/s and $\chi_t = 1.5\,10^{13}$ cm^2/s. This leads to $\Gamma = 3\,10^{11}$ and $\text{Ta} = 3\,10^7$. The stratification of the entire solar convection zone is so large that it cannot be covered with a reasonable grid resolution. In the cases considered below we restrict ourselves to $N_p \approx 7$ and effectively cut off the outer 3% of the solar radius. The volume of the convection zone between $r_0 = 0.7\,R_\odot$ and $R = 0.97\,R_\odot$ is $V = 8\,10^{32}$cm^3 and so the average density is 0.07 g/cm^3 and $\mathscr{L} = 10^6$. We adopt a "surface" temperature at $R = 0.97\,R_\odot$ of $T_S = 1.4\,10^5$ K, taken from a standard mixing length model, which gives $\xi = 0.01$. If we take $\xi_{\text{cor}} = \xi$ then we have $C_\alpha \approx 27$ and $\alpha_B \approx 10^{-5}$. In practice, however, we treat C_α and α_B as free parameters.

© European Southern Observatory • Provided by the NASA Astrophysics Data System

1992A&A...265..328B

2.6. Nondimensional quantities

We introduce nondimensional variables by measuring the radial coordinate r in units of the outer radius R, time t in magnetic diffusion times R^2/η_t, and the density ρ in units of the mean density $\overline{\rho}$. The entropy s is measured in units of c_p. The units for the basic nondimensional variables are:

$$[r] = R, \quad [t] = R^2/\eta_t, \quad [\rho] = \overline{\rho}, \quad [s] = c_p. \tag{21}$$

The units for the other nondimensional variables are

$$[\boldsymbol{u}] = \eta_t/R, \;\; [\boldsymbol{B}] = [\boldsymbol{u}](\mu_0\overline{\rho})^{1/2}, \tag{22}$$

$$[p] = \overline{\rho}[\boldsymbol{u}]^2, \;\; [L] = \overline{\rho}\eta_t^3/R. \tag{23}$$

In summary, 14 parameters are necessary to specify our models: $\xi, \Gamma, \mathscr{L}$, Pr, Pr_M, P_μ, Ta, $r_0, \gamma, V^{(0)}, V^{(1)}, H^{(1)}, C_\alpha, \alpha_B$. Specifying the first three of these is equivalent to specifying the physical parameters T_S, GM, L. Finally, of course, R, η_t, $\overline{\rho}$, c_p in (21) have to be specified to give the basic units, and $\mu_0 = 4\pi$ in Gaussian units. If we regard the basic physical model as being fixed, then 6 quantities ξ, Γ, $\mathscr{L}$, Pr, Pr_M and Ta are necessary to specify the hydrodynamic model, and additionally C_α for the dynamo models. Using solar values from Sect. 2.5 we have

$$[r] = 7\,10^{10}\,\mathrm{cm}, \quad [t] = 31\,\mathrm{yr}, \quad [\rho] = 0.07\,\mathrm{g/cm^3}, \tag{24}$$

$$[\boldsymbol{u}] = 70\,\mathrm{cm/s}, \;\; [\boldsymbol{B}] = 70\,\mathrm{gauss}, \tag{25}$$

$$[p] = 350\,\mathrm{g\,cm^{-1}s^{-2}}, \;\; [L] = 1.3\,10^{26}\mathrm{g\,cm^2s^{-3}}. \tag{26}$$

3. Reformulation of the equations

3.1. The reference state

The equations governing the reference state, Eqs. (12) and (13), in nondimensional form are

$$dp_0/dr = -g\rho_0, \tag{27}$$

$$ds_0/dr = -\mathrm{Pr}_M^2\mathrm{Pr}\mathscr{L}/(p_0 r^2), \tag{28}$$

where

$$g = \mathrm{Pr}_M^2\Gamma/r^2 \tag{29}$$

is the (nondimensional) gravity. The nondimensional luminosity for the reference state is

$$L_0 = 4\pi\mathscr{L}\mathrm{Pr}_M^3/\nabla_{\mathrm{ad}}. \tag{30}$$

In order to satisfy $\overline{\rho} = \int \rho\, dV / \int dV = 1$ we solve Eqs. (27) and (28) iteratively. At each iteration step we integrate these equations inwards, starting at $r = 1$, with $p_0(1) = \xi g(1)\rho_0(1)$, $s_0(1) = \frac{1}{\gamma}\ln p_0(1) - \ln\rho_0(0)$. At each step we update $\rho_0(r)$ using Eq. (10) with $\rho_0(0) = \rho_0(0)^{(\mathrm{old})} V/M_c^{(\mathrm{old})}$.

3.2. The momentum equation

In the anelastic approximation, the toroidal part of the momentum equation is

$$\rho\varpi^2\frac{\partial\Omega}{\partial t} = -\mathrm{div}\,[\rho\varpi^2(\Omega\boldsymbol{u}_p - \mathrm{Pr}_M\nabla\Omega) - \varpi b\boldsymbol{B}_p + \rho\varpi\Omega\boldsymbol{\Lambda}], \tag{31}$$

and the poloidal part can be written in the form

$$\frac{\partial \boldsymbol{m}_p}{\partial t} = -\nabla p_1 + \rho\boldsymbol{f} + \mathrm{Pr}_M\nabla^2\boldsymbol{m}_p, \tag{32}$$

where $\boldsymbol{m} = \rho\boldsymbol{u}$ is the mass flux vector $\rho\boldsymbol{u}$, the suffix p refers to the poloidal (meridional) part of the field, and

$$\rho\boldsymbol{f} = \rho_1\boldsymbol{g} + \rho\boldsymbol{\varpi}\Omega^2 - \boldsymbol{m}_p\cdot\nabla\boldsymbol{u}_p + \boldsymbol{J}\times\boldsymbol{B} - \mathrm{Div}\,(\rho\mathscr{Q}^{(\lambda)}) \tag{33}$$

is the force arising from the presence of rotation, meridional flows and magnetic fields. Here, $\boldsymbol{\varpi} = \varpi(\sin\theta, \cos\theta, 0)$ is the component of the position vector perpendicular to the rotation axis. In (32) and (33) we have subtracted the reference solution and consider deviations denoted by subscript 1.

The diffusive part of $\rho\mathscr{Q}$ can be written in a more compact form by using

$$u_{i,j} = m_{i,j} + \lambda_i m_j, \tag{34}$$

where

$$\boldsymbol{\lambda} = \nabla\ln\rho. \tag{35}$$

In this way we can split $\rho\mathscr{Q}$ into two parts. Since $\boldsymbol{m}_p$ is solenoidal we can treat the term $\nu_t(m_{i,j} + m_{j,i})$ in the same way as in the incompressible case. The divergence of this term simply yields $\nabla^2\boldsymbol{m}_p$ ($\equiv -\mathrm{curl}\,\mathrm{curl}\,\boldsymbol{m}_p$). The diffusive part of the stress tensor which is not included in the term $\mathrm{Pr}_M\nabla^2\boldsymbol{m}_p$ is $\rho\mathscr{Q}_{ij}^{(\lambda)} = \mathrm{Pr}_M(\lambda_i m_j + \lambda_j m_i + P_\mu\delta_{ij}\boldsymbol{\lambda}\cdot\boldsymbol{m})$, where $i, j = r, \theta, \phi$. In these spherical polar coordinates the tensor $\rho\mathscr{Q}_{ij}^{(\lambda)}$ is given explicitly by

$$\rho\mathscr{Q}^{(\lambda)} = \mathrm{Pr}_M\begin{pmatrix} 2\lambda_r m_r & \lambda_r m_\theta + \lambda_\theta m_r & 0 \\ \lambda_r m_\theta + \lambda_\theta m_r & 2\lambda_\theta m_\theta & 0 \\ 0 & 0 & 0 \end{pmatrix} + \mathrm{Pr}_M P_\mu(\boldsymbol{\lambda}\cdot\boldsymbol{m})\boldsymbol{I}, \tag{36}$$

where $\boldsymbol{I}$ is the unit matrix. Note that with axisymmetry, the divergence of a tensor in spherical coordinates can be written as

$$\mathrm{Div}\,(\rho\mathscr{Q}^{(\lambda)}) = \begin{pmatrix} \mathrm{div}\,(\rho\mathscr{Q}^{(\lambda)}\hat{\boldsymbol{r}}) - \frac{1}{r}[\rho\mathscr{Q}_{\theta\theta}^{(\lambda)} + \rho\mathscr{Q}_{\phi\phi}^{(\lambda)}] \\ \mathrm{div}\,(\rho\mathscr{Q}^{(\lambda)}\hat{\boldsymbol{\theta}}) + \frac{1}{r}[\rho\mathscr{Q}_{r\theta}^{(\lambda)} - \rho\mathscr{Q}_{\phi\phi}^{(\lambda)}\cot\theta] \\ 0 \end{pmatrix}, \tag{37}$$

where div is the ordinary divergence operator for vectors in spherical polar coordinates.

3.3. Solving for the pressure

We eliminate the pressure by taking the curl of Eq. (32), which yields

$$(\partial_t - \mathrm{Pr}_M\nabla^2)\boldsymbol{w}_t = \mathrm{curl}\,(\rho\boldsymbol{f}), \tag{38}$$

where $\boldsymbol{w}_t = \mathrm{curl}\,\boldsymbol{m}_p$. However, we need the pressure to compute ρ from Eq. (10). By taking the divergence of Eq. (32) we obtain a Poisson equation for p_1.

© European Southern Observatory • Provided by the NASA Astrophysics Data System

1992A&A...265..328B

$$\nabla^2 p_1 = \mathrm{div}\,(\rho \boldsymbol{f}). \tag{39}$$

We consider impenetrable boundaries, with $\hat{\boldsymbol{r}} \cdot \boldsymbol{m}_p$ vanishing on $r = r_0$, 1. This gives a condition for the pressure:

$$\partial p_1/\partial r = \hat{\boldsymbol{r}} \cdot (\rho \boldsymbol{f} - \mathrm{Pr}_M \mathrm{curl}\, \boldsymbol{w}_t) \quad \text{on} \quad r = r_0, 1. \tag{40}$$

On the axis we have $\partial p_1/\partial \theta = 0$. Thus, the boundary conditions for p_1 are of Neumann-type and p_1 is determined apart from an integration constant $P(t)$, so we write

$$p(r, \theta, t) = p_0(r) + p_1(r, \theta, t) + P(t). \tag{41}$$

$P(t)$ must be determined so as to keep the total mass of the convection zone, M_c, constant; see Sect. 3.6.

3.4. The final set of equations

Since $\boldsymbol{m}$ and $\boldsymbol{B}$ are solenoidal we may express them in the form

$$\boldsymbol{m} = \rho \varpi \Omega \hat{\boldsymbol{\phi}} + \mathrm{curl}\,(\psi \hat{\boldsymbol{\phi}}), \quad \boldsymbol{B} = b \hat{\boldsymbol{\phi}} + \mathrm{curl}\,(a \hat{\boldsymbol{\phi}}). \tag{42}$$

When writing down the equations for the ϕ-components of velocity and vorticity it is convenient to define the Stokes operator, $D^2 a = -\hat{\boldsymbol{\phi}} \cdot \mathrm{curl}\,\mathrm{curl}\,(a\hat{\boldsymbol{\phi}})$. The poloidal parts of $\boldsymbol{m}$ and $\boldsymbol{B}$ are $\boldsymbol{m}_p = \mathrm{curl}\,(\psi\hat{\boldsymbol{\phi}})$ and $\boldsymbol{B}_p = \mathrm{curl}\,(a\hat{\boldsymbol{\phi}})$. The divergence of the poloidal velocity, $\boldsymbol{u}_p = \boldsymbol{m}_p/\rho$, is $\mathrm{div}\,\boldsymbol{u}_p = -\boldsymbol{\lambda} \cdot \boldsymbol{u}_p$. We finally write Eqs. (1), (3), (31), and (38) in the form

$$(\partial_t - D^2) a = \alpha b + \hat{\boldsymbol{\phi}} \cdot (\boldsymbol{u}_p \times \boldsymbol{B}_p), \tag{43}$$

$$\begin{aligned}(\partial_t - D^2) b \; = \; & \alpha j + \hat{\boldsymbol{\phi}} \cdot (\nabla \alpha \times \boldsymbol{B}_p) \\ & - \varpi \boldsymbol{u}_p \cdot \nabla (b/\varpi) + b \boldsymbol{\lambda} \cdot \boldsymbol{u}_p + \varpi \boldsymbol{B}_p \cdot \nabla \Omega,\end{aligned} \tag{44}$$

$$(\partial_t - \mathrm{Pr}_M D^2) w = \hat{\boldsymbol{\phi}} \cdot \mathrm{curl}\,(\rho \boldsymbol{f}), \tag{45}$$

$$\begin{aligned}(\partial_t - \mathrm{Pr}_M \nabla^2)\Omega \; = \; & \mathrm{Pr}_M \nabla \Omega \cdot (\boldsymbol{\lambda} + \boldsymbol{h}) - \frac{1}{\rho \varpi^2} \mathrm{div}\,(\rho \varpi \Omega \boldsymbol{\Lambda}) \\ & - \boldsymbol{u}_p \cdot (\nabla \Omega + \Omega \boldsymbol{h}) + \frac{1}{\rho \varpi^2} \boldsymbol{B}_p \cdot \nabla (\varpi b),\end{aligned} \tag{46}$$

$$\begin{aligned}(\partial_t - \mathrm{Pr}_M \mathrm{Pr}^{-1} \nabla^2) s_1 \; = \; & \mathrm{Pr}_M \mathrm{Pr}^{-1} \nabla \ln p_0 \cdot \nabla s_1 \\ & + (\mathrm{Pr}_M \mathrm{Pr}^{-1} p_0^{-1} \nabla p_1 - \boldsymbol{u}_p) \cdot \nabla s,\end{aligned} \tag{47}$$

where $\boldsymbol{h} = \nabla \ln \varpi^2 = 2\boldsymbol{\varpi}/\varpi^2$. The stream function ψ is given by the solution of

$$D^2 \psi = -w \tag{48}$$

at every time step, and j is given by

$$j = -D^2 a. \tag{49}$$

To sum up we have altogether to solve five equations Eq. (43)-(47), that depend explicitly on time, and two Poisson-type equations (39) and (48), that do not contain the time explicitly.

3.5. Boundary and initial conditions

We assume the outer spherical surface of our computational volume to be surrounded by a vacuum where the current vanishes ($\boldsymbol{J} = 0$), and so the field goes to zero at least as fast as r^{-3}. This leads to

$$b = j = 0 \quad \text{for} \quad r > 1, \tag{50}$$

ie in the entire space outside the sphere, and so our boundary condition at $r = 1$ is $b = 0$. The interior and exterior solutions must be matched such that a and $\partial a/\partial r$ are continuous on $r = 1$. This can be formulated as a nonlocal boundary condition for a on $r = 1$. On the inner boundary we assume a perfect conductor. (For further details see Paper II.) Alternatively, we consider in Sect. 5.8 some cases with a modified lower boundary condition for the magnetic field. The inner and outer boundaries of the shell are taken to be stress free, and thus the fluid boundary conditions become:

$$\left.\begin{aligned}\psi &= 0 \\ \rho r \tfrac{\partial}{\partial r}\left(\tfrac{m_\theta}{\rho r}\right) \equiv \left(\tfrac{2}{r} + \lambda_r\right)\tfrac{\partial \psi}{\partial r} + w &= 0 \\ r \tfrac{\partial \Omega}{\partial r} &= \Lambda_V \Omega\end{aligned}\right\} \text{ on } r = r_0, 1. \tag{51}$$

The boundary conditions for the entropy can be linearized with respect to the reference solution, which gives

$$\frac{\partial}{\partial r} s_1 = -\frac{p_1}{p_0} \frac{d s_0}{dr} \quad \text{on} \quad r = r_0, \tag{52}$$

and

$$\left(\frac{\partial}{\partial r} - b \frac{d s_0}{dr}\right) s_1 = -\frac{p_1}{p_0} \frac{d s_0}{dr} (1 - a - b \nabla_{\mathrm{ad}}) \quad \text{on} \quad r = 1. \tag{53}$$

Assuming as the outer boundary condition a blackbody radiator we have $a = 0$, $b = 4$. Taking instead a fit to the Schwarzschild solution (Sect. 3.5) we have $a = -2$, $b = 8.5$. In the cases considered below we found that the results are not very sensitive to the exact choice of a and b.

3.6. Numerical method

We solve the equations on a r, θ mesh using a DuFort-Frankel scheme for the diffusive terms and second or fourth order (cubic splines) finite differences for the explicit terms on the rhs of Eqs. (43)–(47). The pressure is solved at the beginning of each time step using a decomposition into Legendre polynomials $P_\ell(\cos\theta)$. It turned out that the term $\mathrm{div}\,(\rho_1 \boldsymbol{g})$ on the rhs of (39) can give rise to a numerical instability for strong stratification. Using the linearized equation of state, $\rho_1/\rho_0 \approx p_1/\gamma p_0 - s_1$, we treat the p_1 contribution to the $\rho_1 \boldsymbol{g}$ term implicitly and write

$$\nabla^2 p_1 + \frac{1}{r^2} \frac{\partial}{\partial r} \left(\frac{r^2}{\gamma H_p} p_1\right) = \mathrm{div}\,\left(\rho \boldsymbol{f} + \hat{\boldsymbol{r}} p_1^{(\mathrm{old})}/\gamma H_p\right), \tag{54}$$

where $H_p(r) = p_0/\rho_0 g$ is the local pressure scale height of the hydrostatic reference state and $p_1^{(\mathrm{old})}$ is the value of p_1 from the previous time step.

At each time step we update the pressure offset $P(t)$ in Eq. (41) according to the empirical formula

$$P(t) = P(t - \Delta t) - c_M [M_c(t) - M_c(0)]\, \Gamma \xi / V, \tag{55}$$

© European Southern Observatory • Provided by the NASA Astrophysics Data System

1992A&A...265..328B

Table 1. Relations between various physical phenomena and their related dimensionless parameters. The symbol – stands for absent, × for present, and (×) for optionally present

	Physics			
	α-effect	flows (self-consistent)	stratification	thermal equation
governing parameters	C_α	Ta, Λ	Γ, ξ	$\mathscr{L}$
defining equations	(43), (44)	(45), (46)	(27), (54)	(28), (47)
Model				
unstratified kin. dynamo	×	–	–	–
unstratified diff. rot.	–	×	–	–
unstratified αΛ-dynamo	×	×	–	–
adiabatic stratification	(×)	×	×	–
Boussinesq approximation	(×)	×	–	×
full thermodynamics	(×)	×	×	×

which converges with $M_c(t) \to M_c(0)$ after a number of time steps, provided the coefficient c_M is not too large (we used $c_M = 0.1$).

In most of the cases we use 21 × 21 mesh points in the r and θ directions. In this case we can attain a stratification of about $N_p = 7$ pressure scale height ($\xi = 0.01$). For Ta $= 3\,10^7$, $\Gamma = 3\,10^{11}$, $\mathrm{Pr}_M = 1$, $\mathrm{Pr} = 0.33$ the maximal time step is around 2×10^{-5}, which is similar to the value used previously in the incompressible case. One time step takes about 0.06 seconds on a Convex 220, and a typical run with $3\,10^4$ time steps takes then about 1/2 hour. We repeated some of the most interesting runs with 41 × 41 mesh points. The maximal time step is then 10^{-5}, and takes about 0.23 seconds.

In our program we can gradually change the level of physics involved. For example, at the lowest level we study just kinematical α-effect dynamos, and at the next the Λ-effect with a self-consistent rotation may be included. The effects of gravitational stratification can be included either with energy transport neglected (adiabatic stratification) or included (full thermodynamics). In principle we can also solve the thermal equations neglecting stratification and pressure perturbations (Boussinesq approximation). A summary of these various possibilities and the related dimensionless parameters and equations is given in Table 1.

4. Testing the compressible code

4.1. Adiabatic uniform rotation

In the adiabatic case with rigid rotation ($\Lambda = 0$) no meridional flow should be generated, but the surfaces of constant pressure and density become flattened to oblate ellipsoids. Thus, Eqs. (33) and (38) reduce to $\hat{\boldsymbol{\phi}} \cdot \mathrm{curl}\,(\rho_1 \boldsymbol{g} + \rho\varpi\Omega^2) = 0$, which can be solved using the ansatz $\rho \approx \rho_0(r) + \rho_1(r) P_2(\cos\theta) + ...$, yielding at the surface

$$\frac{\rho_1}{\rho_0} \approx \frac{\Omega^2}{3GMR^2}\frac{d\ln\rho_0}{dr}P_2(\cos\theta) \approx \frac{\mathrm{Ta}}{12\gamma\xi\Gamma}P_2(\cos\theta). \quad (56)$$

For our standard case $\xi = 0.01$, $\Gamma = 3\,10^{11}$, Ta $= 3\,10^7$, the maximal discrepancy arises in the polar regions and is there less than 5%. However, we also find a weak non-vanishing meridional circulation, which is probably due to discretization errors in the scheme. This flow is much smaller than that generated in the presence of a differential rotation (where $\Lambda \neq \mathbf{0}$).

4.2. Boussinesq convection

In the nonadiabatic case we can use the Rayleigh-Bénard instability as a test. Chandrasekhar (1961) gives numerous results for Boussinesq convection where pressure fluctuations are neglected. His model differs from ours, but it can easily be implemented in our code by using $\boldsymbol{g} = -\Gamma \boldsymbol{r}$, $\rho_0 = 1$, $p_1 = 0$, $s_0 = -\frac{1}{2}r^2$ and, as boundary conditions, $s_1 = 0$ on $r = r_0, 1$. His definition of the Rayleigh number corresponds then to Pr Γ. In order to find critical Rayleigh numbers we compute the kinetic energy E_K of the poloidal motions

$$E_K = \tfrac{1}{2}\int \rho \boldsymbol{u}_p^2 dV \quad (57)$$

for weakly supercritical Rayleigh numbers and compute the critical value by extrapolation. When $r_0 = 0.6$ we find for the critical value $\mathrm{Ra}_c \approx 4.14\,10^4$ for 21 × 21 mesh points ($4.09\,10^4$ for 41 × 41 mesh points). This value is less than 2% (0.4%) larger than Chandrasekhar's value ($4.076\,10^4$).

4.3. Stratified convection

Glatzmaier & Gilman (1981) computed critical Rayleigh numbers Ra_c for models with and without rotation and for different degrees of stratification, using $r_0 = 0.6$ with the boundary conditions $T_1 = 0$, ie $s_1 = -\nabla_{\mathrm{ad}} p_1/p_0$, on $r = r_0, 1$. Apart from the fact that Glatzmaier & Gilman also consider nonaxisymmetric modes, our model and definition of Ra should agree with theirs. For Ta = 0 we find $\mathrm{Ra}_c \approx 630$ for the weakly stratified case ($\xi = 40$) and $\mathrm{Ra}_c \approx 870$ for $\xi = 0.01$ (the latter corresponding to $N_p = 8.7$ and $N_\rho = 5$). The marginal Rayleigh numbers of Glatzmaier & Gilman (1981), as determined approximately from their Fig. 2, are smaller by approximately 5% and 17%, respectively. For Ta $= 4\,10^5$ (corresponding to 10^4 with the definition of Glatzmaier & Gilman) we find $\mathrm{Ra}_c \approx 5500$ for $\xi = 40$. This value is about 10% larger than the value for the weakly stratified case shown in Glatzmaier & Gilman. For the case with Ta = 0 and $\xi = 40$ we checked that the discrepancies decrease further if we use 41 × 41 (instead of 21 × 21) mesh points.

We checked that the marginal Rayleigh numbers do not change over a wide range of different values of Γ. We also notice that the results are not very sensitive to $P_\mu = \mu_t/\nu_t$; for example $P_\mu = 0$ instead of −2/3 typically gives 3-5% smaller meridional flow velocities. However, the onset of convection is strongly affected by changing the boundary condition for s_1. For example, using Eqs. (52) and (53) gives $\mathrm{Ra}_c = 150$ (instead of 630) for Ta = 0 and $\xi = 40$. Again, the case with rotation is less

© European Southern Observatory • Provided by the NASA Astrophysics Data System

1992A&A...265..328B

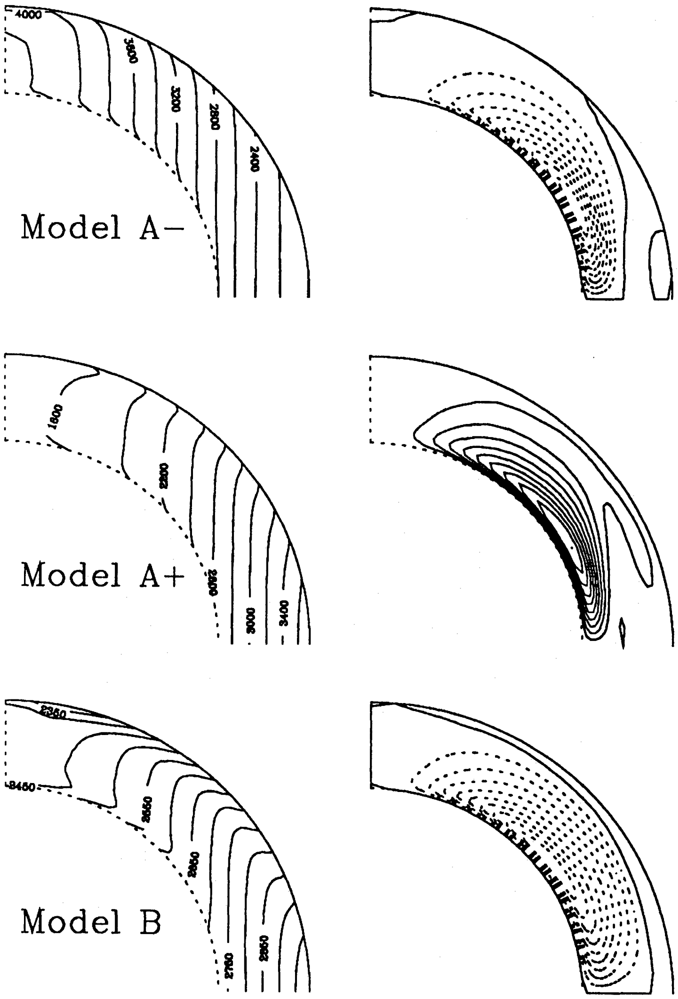

Fig. 1. Angular velocity (on the left) and streamlines of the meridional mass flow (on the right) for cases A$\pm$ (upper two rows) and case B (third row). Dotted streamlines refer to counter clockwise circulation. ($\mathscr{L} = C_\alpha = 0$, Runs n1–n3, adiabatic, no dynamo action)

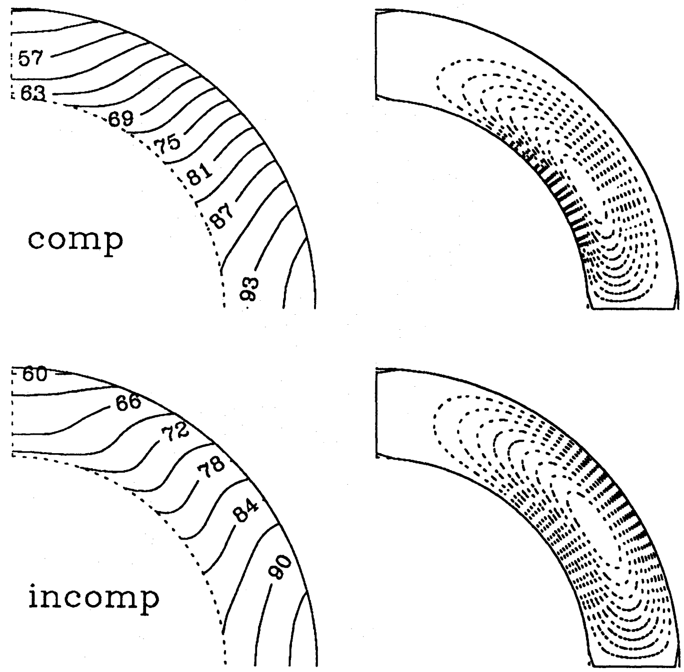

Fig. 2. Angular velocity (on the left) and streamlines of the meridional mass flow (on the right) for case B with Ta $= 3\,10^4$ and $\Gamma = 3\,10^8$. The lower row shows the incompressible unstratifield case for comparison. ($\mathscr{L} = C_\alpha = 0$, adiabatic, no dynamo action)

sensitive and we find $\mathrm{Ra}_c = 5500$, the same value as with the other boundary condition.

We feel that the accuracy of our code is reasonably good for 21×21 mesh points. It might be possible that these test cases could be solved more accurately by using an expansion in terms of Legendre polynomials throughout, although it is not obvious that any such advantage would then carry over to less idealized problems. Moreover, such a technique would adversely affect the ease with which changes and extensions of the code could be made.

5. Results

We now present results using mainly the following parameters: $r_0 = 0.7$, $\mathrm{Ta} = 3\,10^7$, $\Gamma = 3\,10^{11}$, $\xi = 0.01$, $\mathrm{Pr}_M = 1$, $\mathrm{Pr} = 0.33$, and $P_\mu = -2/3$. In some cases we also investigate the cases $\mathrm{Pr} = 0.1$ and 0.2. For the Λ-effect we assume either

$$V^{(0)} = \pm 1,\ V^{(1)} = H^{(1)} = 0 \quad \text{(cases A}\pm\text{)}, \tag{58}$$

which correspond to Kippenhahn's concept of anisotropic viscosity (Rüdiger & Tuominen 1987), and for which we have previously studied dynamos with incompressible flows (Paper II), or

$$V^{(0)} = -1,\ V^{(1)} = H^{(1)} = 5/4 \quad \text{(case B)}, \tag{59}$$

which is believed to represent approximately the solar case (Rüdiger & Tuominen 1990). Here we only consider odd parity (dipole type) magnetic fields and solve the equations in one quadrant of the meridional plane. Of course, some of our solutions may be unstable to magnetic field perturbations of quadrupole symmetry, but the gross properties of dynamos in thin spherical shells are rather similar in the two cases. We first study the adiabatic case s=const, ie $\mathscr{L} = 0$ in Sects. 5.1 and 5.2, and then we include energy transport explicitly in Sects. 5.3 to 5.8.

5.1. The effect of stratification on the rotation law

There are in principle two different ways that a steady meridional flow can conserve mass in the presence of density stratification. If the centre of the circulation pattern lies in the middle of the shell then the velocity in the upper part has to be larger. However, it is also possible that the velocities are similar in the upper and lower parts of the shell, but then the centre of the flow pattern has to be close to the bottom of the convection zone. We find that the latter is the case in most of our models. In Fig. 1 we show the results for the angular velocity and streamlines of meridional flow for different combinations of the Λ-effect parameters (cases A$\pm$ and B) in the absence of magnetic fields ($C_\alpha = 0$). The streamline pattern in all cases looks similar: there is a single circulation cell in the bulk of the convection zone and a more or less clearly defined shallow circulation pattern at low latitudes close to the surface. The Ω-contours are cylindrical (parallel to

© European Southern Observatory • Provided by the NASA Astrophysics Data System

1992A&A...265..328B

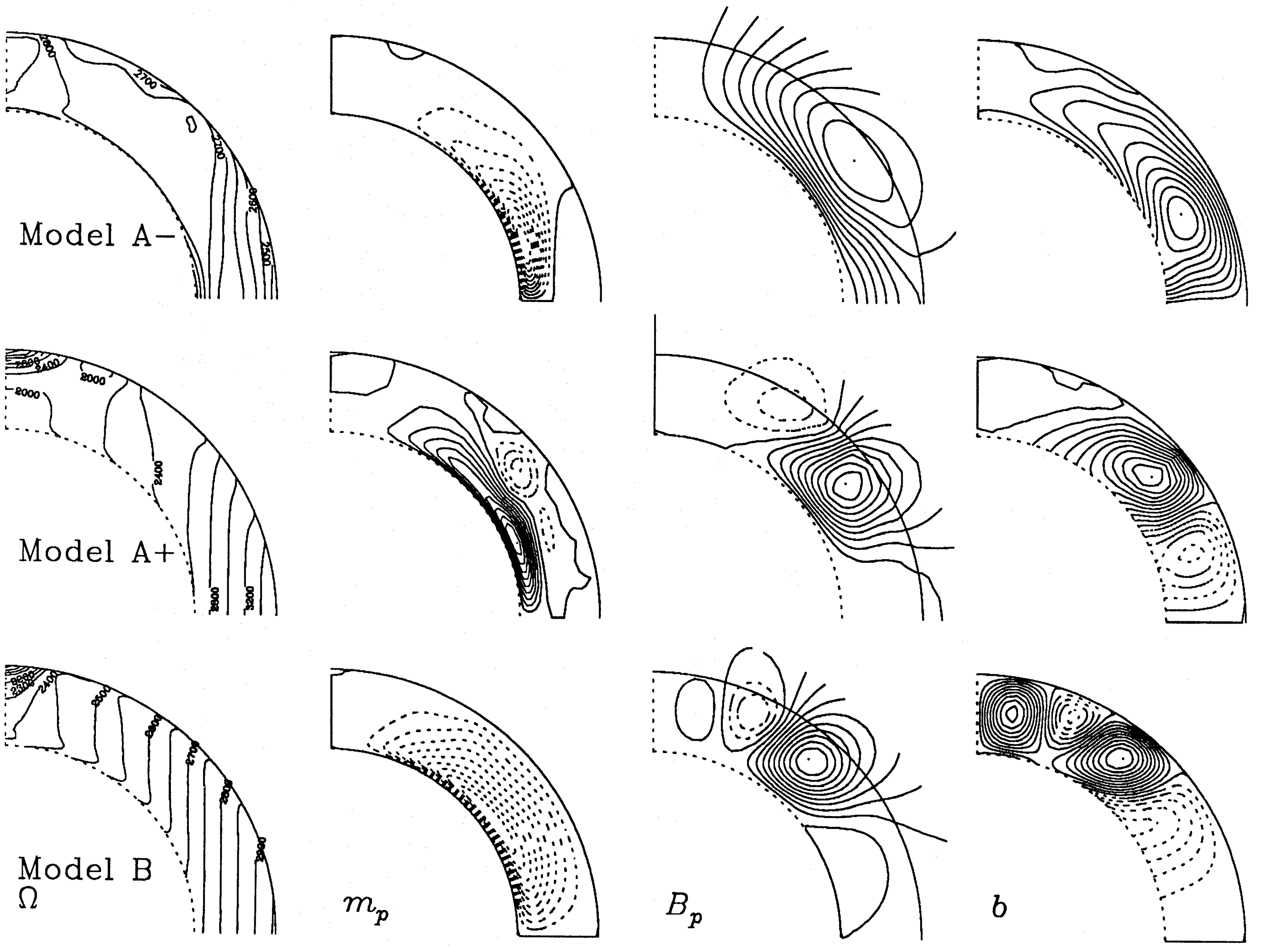

Fig. 3. Contours of angular velocity, streamlines of meridional mass flow, poloidal magnetic field lines and contours of toroidal field, for cases A± (for $C_\alpha = 10$, upper two rows) and case B (for $C_\alpha = 18$, third row). Dotted contours refer to counter clockwise oriented field lines and streamlines or negative toroidal magnetic field. The magnetic field in Model A− is steady (Run N1). In Models A+ (Run N2) and B (Run N3) the field is oscillatory and migrating polewards. The last two snapshots are for the time when E_M is minimal. $\xi = 0.01$, $\mathscr{L} = 0$ (adiabatic)

the rotation axis) in the bulk of the convection zone, with minor deviations especially in case B, where the Ω-contours tend to be perpendicular to the rotation axis in the outer part of the shell.

Only Models A+ and B show an equatorial acceleration, whereas in Model A− the polar regions rotate more rapidly than the equator. All three models disagree with the observed solar internal angular velocity distribution in that the Ω-contours are cylindrical. This is primarily a consequence of the large Taylor number. This can be seen in Fig. 2 where we show the Ω-contours and streamlines of the meridional flow for Model B using a 1000 times smaller Taylor number, $\mathrm{Ta} = 3\,10^4$, keeping the ratio Ta/Γ unchanged, ie $\Gamma = 3\,10^8$. Note that the Ω-contours are now radial in mid-latitudes, in approximate agreement with Ω-contours obtained from recent rotational splitting measurements (Libbrecht 1988). The meridional flow pattern is less strongly concentrated to the bottom of the convection zone than in the case with $\mathrm{Ta} = 3\,10^7$. In the lower row of Fig. 2 we have also plotted the result for the compressible case for the same parameters. Note that the meridional circulation pattern is now shifted somewhat closer to the surface and to higher latitudes.

5.2. The effect of stratification on the dynamo

We now consider the results in the presence of dynamo action ($C_\alpha \neq 0$). In Fig. 3 we show snapshots of dynamo solutions for Models A± and B. We take $C_\alpha = 10$ for the Models A±. Model B is harder to excite and so we take here $C_\alpha = 18$.

Comparing the A+ and A− models, the energy is larger in Model A−, and the Ω-contours are expelled from regions of strong magnetic field, ie Ω-gradients are locally reduced. For the case A+ we find an oscillatory magnetic field with poleward migration (in agreement with the expected behaviour for $\alpha\partial\Omega/\partial r > 0$ in the northern hemisphere). A similar case has been presented in Brandenburg et al. (1991b). During the dynamo cycle there are either one or two toroidal flux belts in each hemisphere. Contours of constant angular velocity are strongly modulated by the time dependent magnetic field. For Model B we find a concentration of magnetic fields in high latitudes. The angular velocity is then strongly reduced close to the poles. Similar results have been obtained previously in the incompressible case, see Paper I.

© European Southern Observatory • Provided by the NASA Astrophysics Data System

1992A&A...265..328B

Table 2. Summary of the different runs. The letters in the first column refer to different runs: with thermodynamics included and standard boundary conditions (T), lower boundary condition modified (B), α-quenching included (Q1: $\alpha_B = 10^{-4}$, Q2: $\alpha_B = 10^{-2}$); for (N) no thermodynamics included; and for (I) incompressibility assumed with $\rho = 1$. Nonmagnetic runs are indicated by lower case letters. Runs h1 and h2 refer to cases with anisotropic heat transfer (h1: $HV^{(1)} = -1.6$, h2: $HV^{(1)} = +1.6$; see Sect. 5.7). The letters in the 2nd column denote Models A$\pm$ or B, except in row L1, where $V^{(0)} = -1.5$; see Sect. 6

Run	"Λ"	C_α	Pr	$\mathscr{L}$	C_Ω	$\lg E_K$	$u_\theta^{\max}$	$\lg E_M$	E_M^{pol}/E_M	δU	δL	T_{cyc}
T1	A−	2	0.33	$1.3\,10^5$	−750	2.13	32	4.26	0.009	0	0	st.
T2	A−	5	0.33	$1.3\,10^5$	−628	2.36	44	4.21	0.042	0	0	st.
T3	A−	10	0.33	$1.3\,10^5$	−471	2.41	48	4.03	0.27	0	0	st.
T4	A−	10	0.20	10^6	−482... − 450	2.65...2.68	250...350	4.07	0.28	0	0	st.
T5	A−	10	0.10	10^6	−474	2.40	46	4.03	0.27	0	0	st.
T6	A−	15	0.10	10^6	−403	2.40	44	4.08	0.55	0	0	st.
T7	A+	10	0.10	10^6	+993... + 1010	1.65...1.74	22...122	3.77...3.90	0.05...0.08	10^3	30	0.041
T8	A+	−10	0.10	10^6	+942	2.06	48	4.07	0.09	0	0	st.
T9	B	18	0.10	10^6	+238... + 239	1.06...1.07	22...25	2.38...2.50	0.31...0.39	50	1	0.10
B1	A−	10	0.10	10^6	−550... − 675	2.21...2.25	45...87	3.68...3.94	0.08...0.10	10^4	300	0.10
B2	A−	10	0.10	10^6	−464... − 645	2.24...2.34	41...102	3.82...4.11	0.06...0.10	$6\,10^3$	200	0.09
Q1	A−	10	0.10	10^6	−665	2.34	46	4.20	0.038	0	0	st.
Q2	A−	10	0.10	10^6	−810	1.67	19	3.42	0.002	0	0	st.
L1	A−	1	0.33	$1.3\,10^5$	−1142	2.48	46	4.56	0.003	0	0	st.
N1	A−	10	no thermo		−481	2.40	44	4.02	0.26	–	–	st.
N2	A+	10	no thermo		+992... + 1006	1.65...1.74	22...94	3.77...3.90	0.05...0.07	–	–	0.041
N3	B	18	no thermo		+238... + 239	1.05...1.06	10...11	2.39...2.50	0.31...0.39	–	–	0.10
I1	A−	10	incompr.		−706	2.09	71	4.05	0.07	–	–	st.
I2	A+	10	incompr.		+886... + 893	1.25...1.31	21...23	3.51...3.61	0.06...0.08	–	–	0.043
I3	B	18	incompr.		+233... + 239	0.96...0.97	10...11	2.49...2.65	0.32...0.42	–	–	0.060
I4	B	−10	incompr.		+218	0.88	12	3.06	0.17	–	–	st.
t1	A−	0	0.10	10^6	−813	1.65	19	–	–	–	–	–
t2	B	0	0.33	$1.3\,10^5$	265	1.07	11	–	–	–	–	–
h1	B	0	0.33	$1.3\,10^5$	271	1.18	12	–	–	–	–	–
h2	B	0	0.33	$1.3\,10^5$	260	0.95	9	–	–	–	–	–
n1	A−	0	no thermo		−810	1.65	18	–	–	–	–	–
n2	A+	0	no thermo		+1110	1.22	27	–	–	–	–	–
n3	B	0	no thermo		+265	1.07	11	–	–	–	–	–

Some relevant parameters for a number of runs are summarized in Table 2. As in Paper II we measure the strength of the Ω-effect by the equatorial angular velocity difference $C_\Omega = \Omega(1, \pi/2) - \Omega(r_0, \pi/2)$. The magnitude of this quantity is often found to be more important for the presence of dynamo waves than, for example, the latitudinal angular velocity difference. We also determine the (dimensionless) magnetic energy in the convection zone,

$$E_M = \frac{1}{2} \int \boldsymbol{B}^2 dV, \tag{60}$$

and the strength of the poloidal magnetic energy relative to the total magnetic energy, E_M^{pol}/E_M. The period of the magnetic cycle is T_{cyc}.

The marginal values of C_α for dynamo action vary considerably in the three models (below 2 for Model A−, below 10 for Model A+, and somewhat below 18 for Model B). Note that the total magnetic energy can actually decrease with C_α (see cases T1–T3 in Table 2), and that only the energy of the poloidal magnetic field increases (approximately linearly) with C_α.

The dynamo period for Model A+ is not very different between the compressible and the incompressible cases (compare Run T7 and N2 with I2). For Model B, however, the period is in the compressible case almost twice as long as in the incompressible case (compare Runs T9 and N3 with I3).

We did not find oscillatory solutions either for Model A− with $C_\alpha > 0$ or Model B with $C_\alpha < 0$. If the Ω-effect was larger, ie Ta or Pr_M larger, then the dynamo would become oscillatory. In Paper II we only found oscillatory solutions for $\mathrm{Ta} \geq 5\,10^7$ (Model A− with $\mathrm{Pr}_M = 1$). We note, however, that during the growth phase of the dynamo the $E_M(t)$ curve shows a weak oscillatory modulation, which disappears as the dynamo saturates. Two computations for Model A− with α-quenching included suggest that the nature of the nonlinearity ($\alpha_B = 10^{-4}$ in Run Q1 and 10^{-2} in Run Q2) is not crucial for the existence of steady behaviour.

We compare the compressible and incompressible Models A+ for $C_\alpha = 10$ (Runs N2 and I2) by plotting for different time steps the radial dependence of magnetic energy density and kinetic energy densities from the poloidal motions, averaged over spherical shells, i.e. $\langle \frac{1}{2}\boldsymbol{B}^2 \rangle$, and $\langle \frac{1}{2}\rho \boldsymbol{u}_p^2 \rangle$; see Fig. 4. Here, angular brackets denote $\langle f \rangle = \frac{1}{2} \int f \sin\theta d\theta$. Note that the profiles of the magnetic energy density are not much altered in the presence of stratification. In the stratified case the meridional

© European Southern Observatory • Provided by the NASA Astrophysics Data System

1992A&A...265..328B

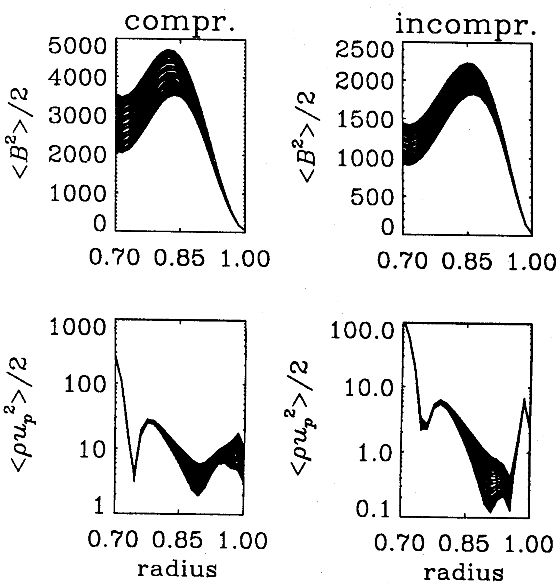

Fig. 4. $\langle \frac{1}{2}\boldsymbol{B}^2 \rangle$ and $\langle \frac{1}{2}\rho \boldsymbol{u}_p^2 \rangle$ for the compressible and incompressible case (Runs N2 and I2). A number of profiles for different time steps have been superimposed in order to show the cyclic variation in different layers

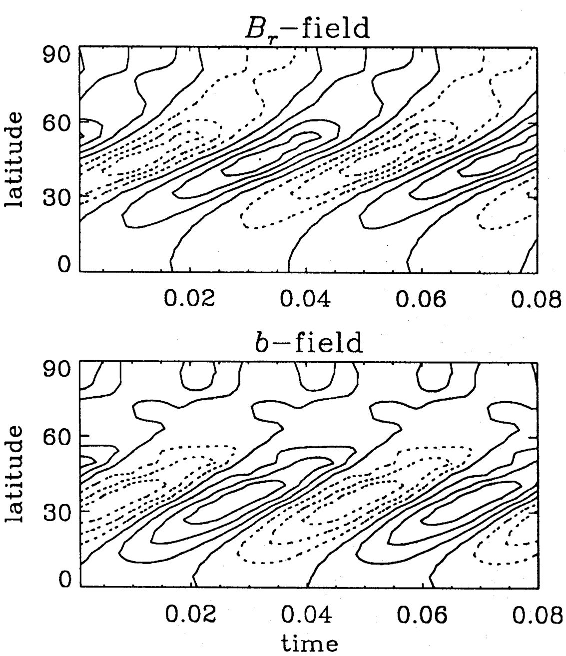

Fig. 5. Butterfly diagrams of the B_r-field at $r = 1$ (upper panel) and the B_ϕ-field at $r = 0.985$ (lower panel) for Model A+ with $C_\alpha = 10$ (Run N2, adiabatic)

flow and its temporal variation are somewhat larger than without stratification, especially in the upper layers where ρ is small and the Lorentz force per unit mass, $\boldsymbol{J} \times \boldsymbol{B}/\rho$, large.

Butterfly diagrams for the B_r- and B_ϕ-fields (taken immediately below the surface) are shown in Fig. 5 for Run N2. The toroidal field is more concentrated to the equator than B_r. Dynamo waves migrate polewards – in agreement with the expected behaviour for $\alpha\partial\Omega/\partial r > 0$.

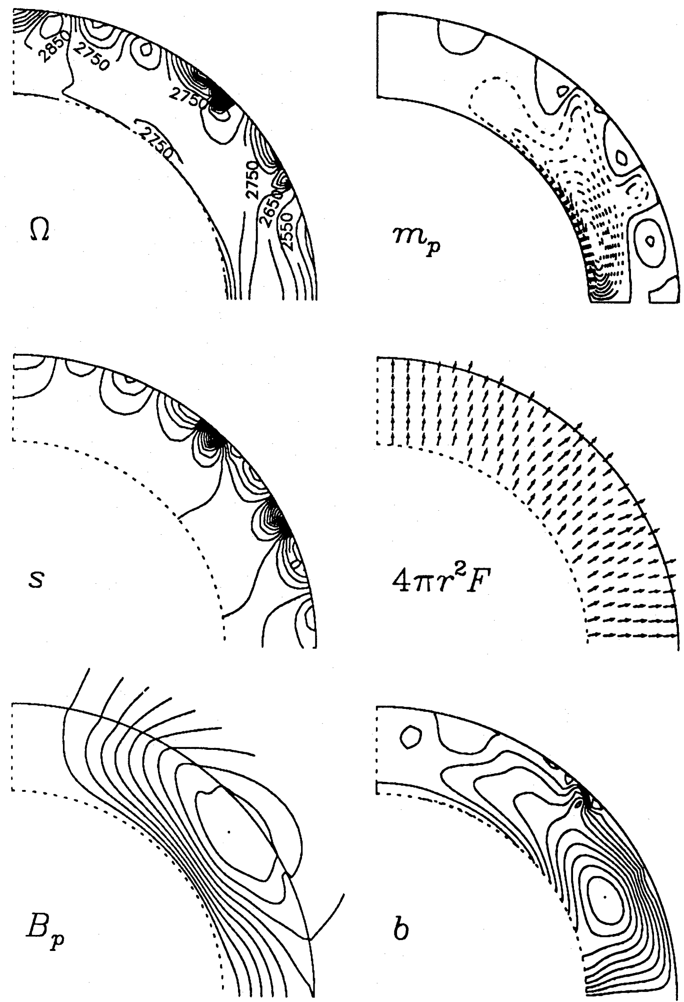

Fig. 6. Contours of angular velocity Ω, streamlines of meridional mass flow ($\boldsymbol{m}_p$), contours of entropy perturbation s_1, vectors of normalized convective flux $4\pi r^2 \boldsymbol{F}^{\rm conv}$, poloidal magnetic field lines ($\boldsymbol{B}_p$), and contours of toroidal field (b), for a slightly supercritical Rayleigh number. Pr=0.2, Ra=7000, Model A−, $C_\alpha = 10$, $\xi = 0.01$, $\mathscr{L} = 10^6$ (Run T4, nonadiabatic, dynamo)

5.3. *Nonadiabatic effects*

We now investigate the nonadiabatic case $\mathscr{L} \neq 0$. The possibility of the onset of large scale Rayleigh-Bénard convection (see Sect. 4.3), as opposed to the small scale convection modelled in terms of turbulent transport coefficients, restricts our "choice" of the parameters Pr and $\mathscr{L}$. For Pr = 0.33 and $\mathscr{L} = 10^6$ the turbulent Rayleigh number is around 10^4, which is already supercritical and leads to the onset of large scale Rayleigh-Bénard convection. (The critical turbulent Rayleigh number is in the presence of Λ-effect and magnetic fields around 5000.)

Clearly, a model with prescribed values for ν_t and χ_t, independent of the *actual* entropy gradient, is unrealistic. According to mixing length theory the turbulent diffusivity adjusts itself and increases as the entropy gradient becomes steeper. Also the flow may become nonaxisymmetric (e.g. Glatzmaier & Gilman 1981), although our model differs from theirs in several respects, and we have not performed the corresponding stability analysis. If this were to happen then, of course, conclusions based on an

© European Southern Observatory • Provided by the NASA Astrophysics Data System

1992A&A...265..328B

axisymmetric model will be meaningless. It is not the aim of this paper to address this general problem any further. Since there is also no sufficient observational evidence for such a large scale convective flow, we consider primarily the case of slightly subcritical $\mathscr{L}$, and so we take in the following either $\mathscr{L} = 1.3 \times 10^5$, or we lower the Prandtl number and use $\mathrm{Pr} = 0.1$ and $\mathscr{L} = 10^6$. However, we also consider one case with a slightly supercritical Rayleigh number using $\mathrm{Pr} = 0.2$ and $\mathscr{L} = 10^6$ (Run T4).

The effects of thermodynamics on the dynamo are weak if the Rayleigh number is subcritical; compare the dynamo runs in Table 2 without thermodynamics (Runs N1–N3) and those with thermodynamics included (Pr=0.1 and Ra=1700; Runs T5, T7, T9). For supercritical Rayleigh numbers (Pr=0.2, Ra=7000; Run T4) the meridional flow at the surface is very large ($u_\theta \approx 300$), even though the kinetic energy of the meridional motions is not much increased. In this case (Run T4) the flow in the uppermost layers remains time dependent. (For this run we used a resolution of 41×41 mesh points.) A snapshot of the flow and field pattern is shown in Fig. 6. The magnetic field is practically steady, but the flow (Ω and $\boldsymbol{m}_p$) varies strongly with time at the surface. Vectors of the normalized convective flux $4\pi r^2 \boldsymbol{F}^{\mathrm{conv}}$ show noticeable deviations from the radial direction. The flow pattern is of small scale and it is possible that it would be unstable to nonaxisymmetric perturbations. In this connection it is important to recall that the magnetic field, generated by a mean-field dynamo in the presence of sufficiently strong differential rotation, is expected to be stable to nonaxisymmetric perturbations (Jennings et al. 1990). Our assumption of axisymmetry is therefore reasonable in the case of subcritical Rayleigh numbers.

For Model A− with $C_\alpha > 0$ we find only steady solutions for a broad range of C_α (Runs T1–T6). In order to study oscillatory solutions we now consider Model A+. In Fig. 7 we show cross sections of the poloidal and toroidal magnetic fields, meridional flow, angular velocity and entropy perturbation for the oscillatory Model A+ with $C_\alpha = 10$ (Run T7) for half a magnetic cycle. The magnetic field consists mainly of two poleward migrating toroidal flux belts of opposite polarity. The shape of the Ω-contours is only weakly affected by the magnetic field. This is also reflected by the relatively small cyclic variation of C_Ω in this case (see Table 2). The meridional flow is divided mainly into two counter rotating cells which vary with time. The contours of s_1, entropy perturbation, show a small scale pattern that changes rapidly with time, especially close to the surface.

For oscillatory models the cyclic variation of the magnetic pressure is approximately three times smaller than the variation of the gas pressure. This indicates that the two are not in balance as it is typically found in compressible hydromagnetic dynamo simulations (Nordlund et al. 1992), where no mean-field assumption is made nor α-effect assumed. In our mean field model the gas pressure modulation presumably arises not from the approximate equilibrium of magnetic and gas pressures, but mainly from the significant cyclic variation of the angular velocity.

5.4. Meridional flow and magnetic field strength

Using the units for velocity and magnetic field defined in Eq. (25) we find that in the nonmagnetic cases $u_\theta^{\max}$ ranges from 8 m/s (Model B) to 20 m/s (Model A+). In the magnetic case $u_\theta^{\max}$ may reach values around 30–40 m/s if the dynamo is steady, but may vary in the range 20–80 m/s in the oscillatory case (Run T7).

In the bulk of the convection zone the dimensionless value of $\frac{1}{2}\langle \boldsymbol{B}^2 \rangle$ is typically around 4000 (see Fig. 4) which corresponds to a magnetic field strength of about 6 kgauss. This is comparable with the equipartition value of about 5 kgauss (Durney et al. 1990). This value is consistent with the estimate

$$B_{\mathrm{eq}} = u_t(\mu_0 \bar{\rho})^{1/2} \approx (3\eta_t/\ell_{\mathrm{cor}})(\mu_0\bar{\rho})^{1/2} = 3[\boldsymbol{B}]\xi_{\mathrm{cor}}^{-1}, \tag{61}$$

if $\ell_{\mathrm{cor}} \approx 30\,\mathrm{Mm}$ ($\xi_{\mathrm{cor}} = 0.04$) is assumed. This value of ξ_{cor} is larger than the value corresponding to $C_\alpha = 10$ ($\xi_{\mathrm{cor}} \approx 2C_\alpha/\mathrm{Pr}_M \mathrm{Ta}^{1/2} = 3\,10^{-3}$; see Sect. 2.4), but but these estimates are anyway rather uncertain.

Schüssler (1979) presented compressible, but isothermal, mean-field dynamo models with density stratification and feedback from the Lorentz force of the mean magnetic field. He found peak values of 200 gauss for the magnetic field and 2 m/s for the flow, that are at least one order of magnitude smaller than in our model. However, the ratio of kinetic to magnetic energies in Schüssler's models is around 0.03, which is close to our values for E_K/E_M; see Table 2.

5.5. Luminosity variations

In Model A+ with $C_\alpha = 10$, $\mathscr{L} = 10^6$ and $\mathrm{Pr} = 0.1$ the dimensionless luminosity is 3×10^7 (see Eq. (30)) and the cyclic luminosity variation is about 30 (see Table 2), so $\delta L/L = 10^{-6}$. The luminosity variation δL_m at the mean radius of the shell, r_m, is much larger. We find $\delta L_m \approx 1.5\,10^4$ and $\delta L_m/L \approx 5\,10^{-4}$. In Fig. 8 we plot the cyclic variations of magnetic and thermal energies, δE_M and δU, respectively, and compare with the variations in luminosity at $r = 1$ and $r = r_m$. Note that δU is of similar order of magnitude as δE_M. Maxima of δU occur shortly after minima of δE_M and δL lags δE_M by $0.12\,T_{\mathrm{cyc}}$, whilst δE_M and δL_m are approximately in phase.

In Model B with $C_\alpha = 18$, the magnetic energy is much smaller than in Model A+ with $C_\alpha = 10$, but $\delta E_M = 70$ and $\delta U = 50$ are still of similar order of magnitude, and the luminosity variations are smaller ($\delta L = 1$ and $\delta L_m = 160$); see Table 2. The small surface value of $\delta L/L$ may be a consequence of the boundary condition for s_1, even though $\delta L/L$ does not change significantly for different pairs of the exponents a, b in Eq. (53).

Cyclic variations of the solar luminosity have been theoretically predicted by Spiegel & Weiss (1980). They find that substantial variations arise from changes in the adiabatic temperature gradient $(\partial T/\partial r)_{\mathrm{ad}}$, which enters directly into the equation for the convective energy flux. This can be written, using Eqs. (9) and (10), as

$$F^{\mathrm{conv}} = \chi_t \rho c_p \left[\frac{\partial T}{\partial r} - \left(\frac{\partial T}{\partial r}\right)_{\mathrm{ad}}\right]. \tag{62}$$

Spiegel & Weiss show (Eqs. (5) and (7) in their paper) that the change of thermal energy U in the convection zone is

$$\delta U \sim c_p \delta \left(\frac{\partial T}{\partial r}\right)_{\mathrm{ad}} M_c d \sim \delta E_M, \tag{63}$$

where $U = \int \rho c_v T\,dV = (\gamma - 1)^{-1} \int p\,dV$. Our computations confirm that the variations of δE_M and δU are indeed of the same order of magnitude; see Fig. 8. Spiegel & Weiss argue further that these variations affect the convective flux and that such modifications reach the surface in a few months. They expect variations of the luminosity to be of the order of the rate of magnetic energy variation, $\delta E_M/\tau$, where $\tau \approx T_{\mathrm{cyc}}/4 \approx 6\,\mathrm{yr}$ for the Sun.

© European Southern Observatory • Provided by the NASA Astrophysics Data System

1992A&A...265..328B

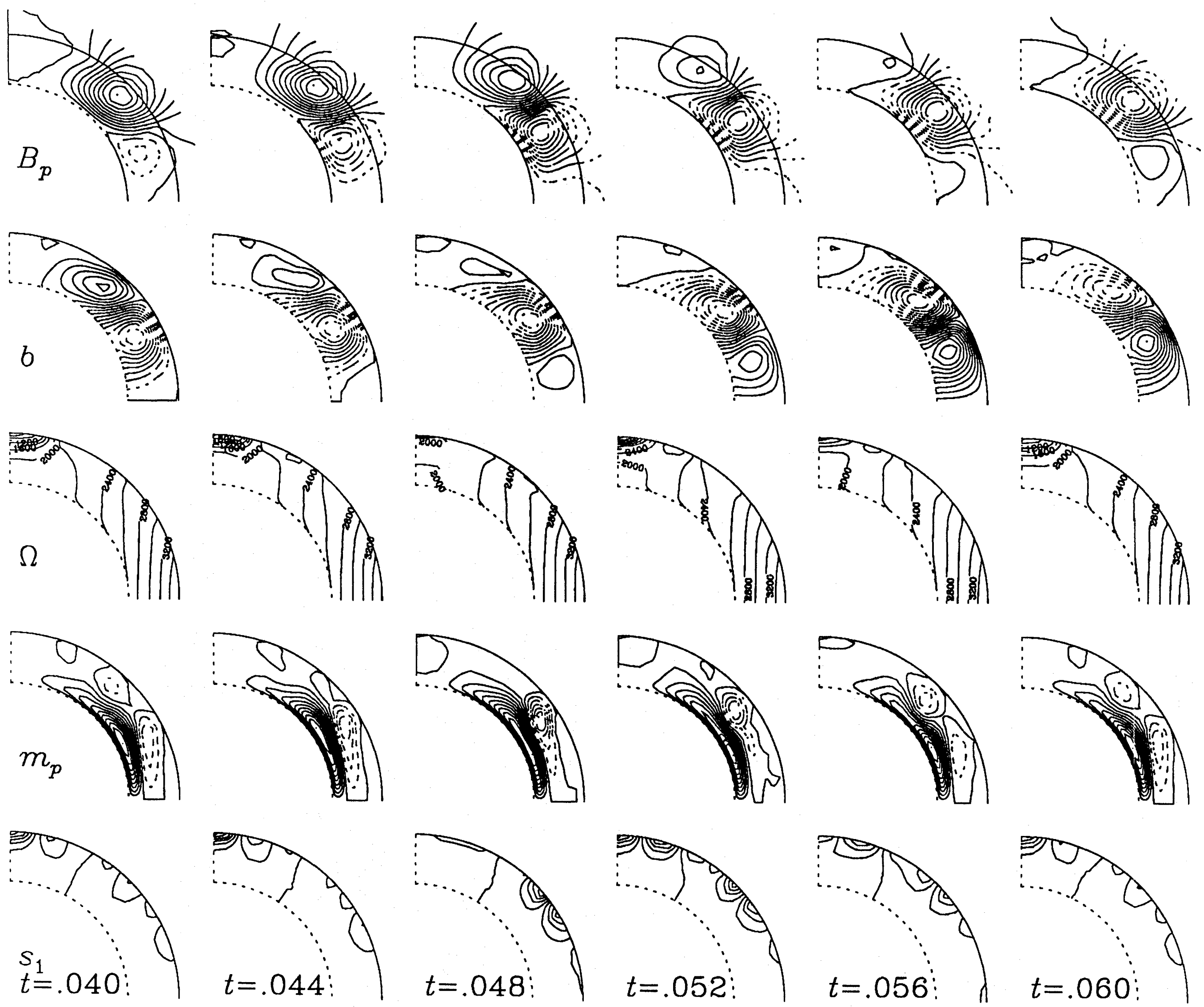

Fig. 7. Snapshots of poloidal magnetic field lines (first row), contours of toroidal field (second row), contours of angular velocity (third row), streamlines of meridional mass flow (fourth row), and contours of entropy perturbation (last row). Dotted contours refer to counter clockwise oriented field lines and streamlines or negative toroidal magnetic field. The maximum and minimum of E_M occur respectively at $t = 0.044$ and 0.054. Model A+, $\xi = 0.01$, $\mathscr{L} = 10^6$ (Run T7, nonadiabatic, dynamo)

In our model both $\delta E_M/\tau$ and $\delta U/\tau = O(10^7)$ are of the order 10^7, which is much larger than δL. In deeper layers the variation of luminosity is larger (of the order of 10^4), but it is still small compared with the rate of energy variation. This means that in our model a substantial amount of magnetic and thermal energy is converted into other forms of energy, most notably the rotational energy. The situation might be quite different if the feedback on the α effect was included so that the cyclic variations of Ω were smaller.

5.6. Thermal shadows

Parker (1987) proposed that thermal shadows above flux tubes might lead to a substantial cooling above them associated with a downflow. This downflow might counteract the effects of magnetic buoyancy. A similar mechanism ("negative buoyancy") has recently been investigated by Vainshtein & Levy (1991).

In order to investigate this mechanism in our model we consider the variation of the convective flux and the vertical velocity by plotting "butterfly diagrams" of $F_r^{\rm conv}$ and u_r at $r = r_m$; see Fig. 9. Note that the times and latitudes of large magnetic energy density coincide approximately with those of smaller convective flux accompanied by negative radial velocities (downflows). Thus, we confirm the general idea of thermal shadows. It is not obvious, however, to what extent these downflows also contribute to pushing the flux tubes down.

5.7. Anisotropic heat transport

Stix (1989) pointed out that a sufficiently large latitudinal entropy gradient might significantly relax the conditions under which

© European Southern Observatory • Provided by the NASA Astrophysics Data System

1992A&A...265..328B

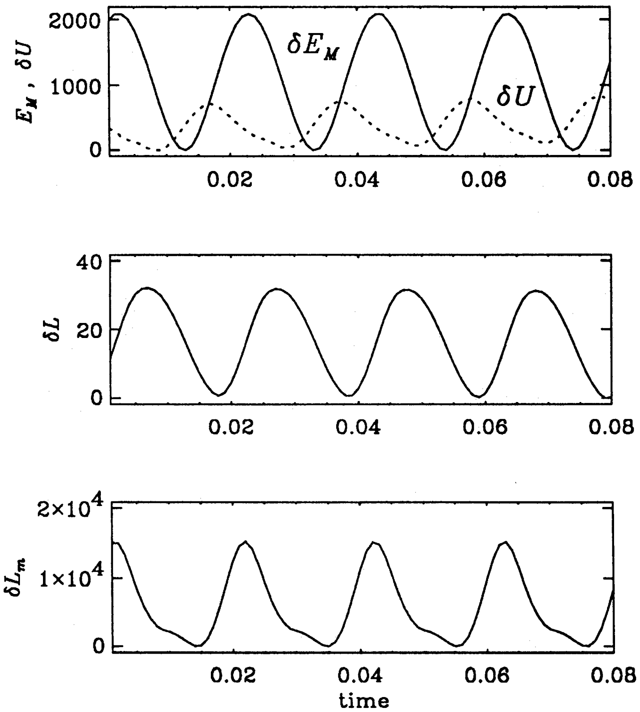

Fig. 8. Variation of magnetic and thermal energies (upper panel), and luminosity at the surface (second panel) and in the middle of the shell (third panel). In all panels deviations of quantities from their minimum values are plotted

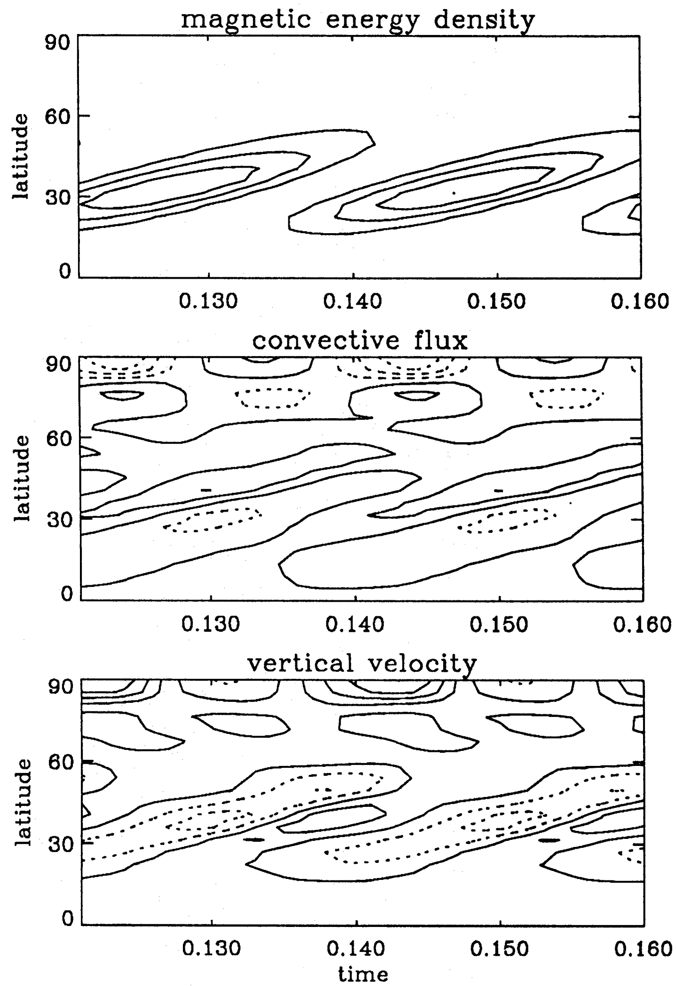

Fig. 9. Butterfly diagrams of $\boldsymbol{B}^2$, $F_r^{\rm conv}$, and u_r at $r = r_m = 0.85$. In the middle panel dotted contours indicate that the convective flux is smaller than the average. In the last panel negative values of u_r (downflows) are shown as dotted contours

the Taylor-Proudman theorem applies. In order to quantify this possibility we now consider a simple form of anisotropic heat conductivity, following Rüdiger (1989),

$$\chi_{ij} = \chi_t[\delta_{ij} - \delta_{i\theta}\delta_{jr}\sin\theta\cos\theta HV^{(1)}], \tag{64}$$

where $HV^{(1)}$ is a dimensionless number characterizing the magnitude of the horizontal flux due to a vertical entropy gradient. The second term in Eq. (64) leads to an additional term on the right hand side of the entropy equation:

$$-HV^{(1)}\left[\frac{1}{p_0 r}\frac{\partial p_1}{\partial\theta}\sin\theta\cos\theta\frac{\partial s}{\partial r} + \mathrm{div}\left(\hat{\boldsymbol{\theta}}\sin\theta\cos\theta\frac{\partial s}{\partial r}\right)\right]. \tag{65}$$

This term gives rise to a systematic latitudinal entropy gradient. Since $\partial s/\partial r < 0$ and $r\mathrm{div}\,(\hat{\boldsymbol{\theta}}\sin\theta\cos\theta) = 3\cos\theta^2 - 1$ this term is positive close to the poles and negative close to the equator, and we expect s to be enhanced close to the poles for $HV^{(1)} > 1$ and enhanced close to the equator for $HV^{(1)} < 1$. Note that an isotropic latitudinal dependent eddy heat conductivity has previously been invoked to explain the solar differential rotation (e.g. Weiss 1965; Durney & Roxburgh 1971). Here, however, we still retain the Λ-effect.

In Fig. 10 we show the resulting Ω-contours and vectors of $4\pi r^2\boldsymbol{F}^{\rm conv}$ in a meridional plane for $HV^{(1)} = \pm 1.6$ and compare with the isotropic case $HV^{(1)} = 0$. We find significant deviations from cylindrical Ω-contours if $|HV^{(1)}| > 1$. At the bottom of the convection zone the convective flux in the latitudinal direction is much larger than in the radial direction when $|HV^{(1)}| > 1$. Nevertheless, the observable flux at the surface remains almost uniform (cf. Spruit 1977), but this may be due to the over simplified upper boundary condition adopted.

We define the relative pole-equator temperature difference as

$$\Delta_T = (T_{\rm pole} - T_{\rm equ})/T_{\rm equ}, \tag{66}$$

evaluated along an equipotential surface close to $r = R$. For the three models we find the following values of Δ_T: 10^{-6} for $HV^{(1)} = -1.6$, $3\,10^{-6}$ for $HV^{(1)} = 0$, and $5\,10^{-6}$ for $HV^{(1)} = +1.6$, ie Δ_T is positive and smallest for negative values of $HV^{(1)}$. If Δ_T was evaluated at $r = R$ (ie not along an equipotential surface) then the result would be quite different (ca. $-5\,10^{-4}$), but this is mainly due to the oblateness caused by the centrifugal force.

Finally, we investigate the vertical dependence of the superadiabatic gradient

$$\Delta\nabla = (\partial s/\partial r)/(\partial\ln p/\partial r), \tag{67}$$

which is listed for the case $HV^{(1)} = 0$ as a function of radius; see Table 3. In the models with $HV^{(1)} = \pm 1.6$ the superadiabatic gradient varies significantly with latitude. In Table 3 we give in the last three columns the relative pole-equator difference of $\Delta\nabla$, ie

$$\Delta_{\Delta\nabla} = (\Delta\nabla_{\rm pole} - \Delta\nabla_{\rm equ})/\Delta\nabla_{\rm equ}. \tag{68}$$

© European Southern Observatory • Provided by the NASA Astrophysics Data System

1992A&A...265..328B

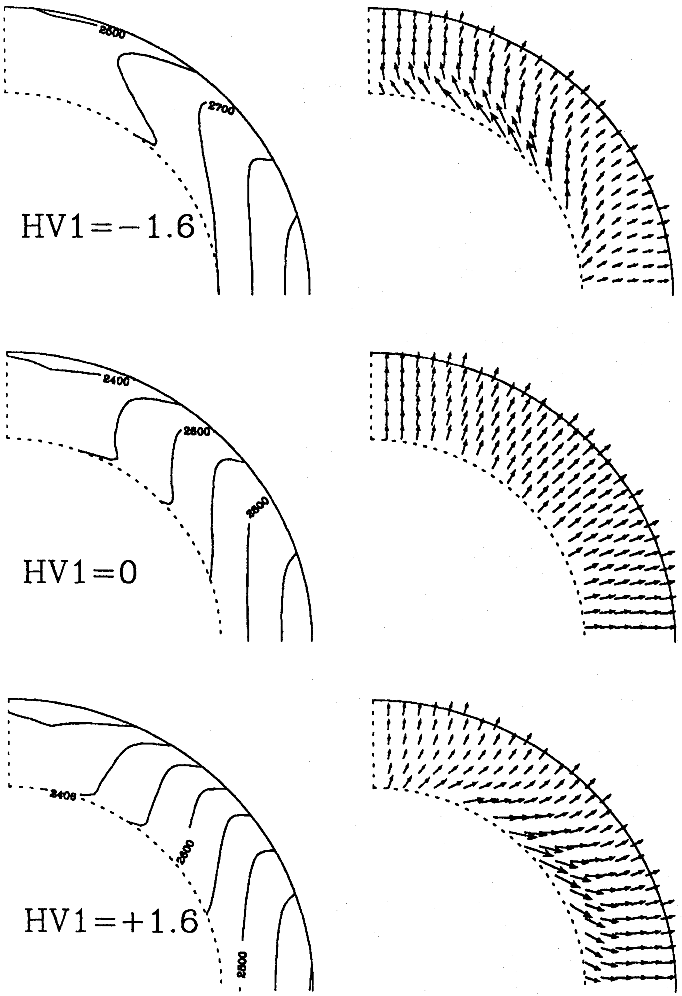

Fig. 10. Ω-contours and vectors of $4\pi r^2 \boldsymbol{F}^{\rm conv}$ in a meridional plane for $HV^{(1)} = -1.6$ (upper row), 1.6 (lower row), and 0, ie the isotropic case (middle row). Pr=0.10, $\mathscr{L} = 10^6$

For $HV^{(1)} = +1.6$ this quantity is negative throughout most of the convection zone, and positive for $HV^{(1)} = -1.6$. Thus, for positive (negative) values of $HV^{(1)}$ the superadiabatic gradient is reduced at the poles (equator). This is also seen in Fig. 10 where the vectors of convective flux are shorter at the poles (equator).

For $HV^{(1)} = -1.6$ the superadiabatic gradient is at the poles twice as big as at the equator. Modifications to the superadiabatic gradient of comparable magnitude were proposed by Weiss (1965) to explain the solar differential rotation.

5.8. *Treatment of the lower boundary*

The assumption of a perfect conductor boundary condition for the magnetic field at the bottom of the convection zone is rather crude and restrictive. (See also the discussion in Moss et al. 1990b.) In particular, the question of whether or not the solutions are oscillatory crucially depends on the lower boundary condition for the magnetic field. The perfect conductor boundary condition may be inadequate, because in reality both poloidal and toroidal magnetic fields will penetrate to some extent into the interior.

In order to illustrate the robustness of our results to this uncertainty we now consider briefly another reasonable possibility

Table 3. Depth dependences of $\Delta_{\Delta\nabla}$ for Model B with $HV^{(1)} = 0$ (i), -1.6 (ii), and $+1.6$ (iii). The fourth column gives the value of $\Delta\nabla$ in the equatorial plane for $HV^{(1)} = 0$. Density and pressure of the reference solution are also given

r	ρ_0	p_0	$\Delta\nabla_{\rm equ}$	(i)	(ii)	(iii)
1.00	0.042	$1.2\,10^8$	$3.4\,10^{-6}$	-0.000	-0.00	0.00
0.97	0.141	$9.5\,10^8$	$1.0\,10^{-6}$	-0.003	0.12	-0.11
0.94	0.281	$3.0\,10^9$	$5.0\,10^{-7}$	-0.000	0.28	-0.22
0.91	0.463	$6.9\,10^9$	$3.0\,10^{-7}$	0.008	0.47	-0.31
0.88	0.687	$1.3\,10^{10}$	$2.0\,10^{-7}$	0.019	0.67	-0.38
0.85	0.957	$2.3\,10^{10}$	$1.5\,10^{-7}$	0.030	0.85	-0.43
0.82	1.279	$3.8\,10^{10}$	$1.1\,10^{-7}$	0.038	0.98	-0.45
0.79	1.659	$5.8\,10^{10}$	$8.3\,10^{-8}$	0.043	1.00	-0.43
0.76	2.103	$8.6\,10^{10}$	$6.6\,10^{-8}$	0.042	0.87	-0.38
0.73	2.623	$1.2\,10^{11}$	$5.3\,10^{-8}$	0.032	0.54	-0.25
0.70	3.228	$1.8\,10^{11}$	$4.3\,10^{-8}$	-0.001	-0.00	-0.01

for the lower boundary condition. Since the solar interior has a finite .uuctivity the magnetic field will penetrate some distance before it vanishes. This suggests using as boundary conditions for a and b

$$\partial a/\partial r = a/\delta_a, \quad \partial b/\partial r = b/\delta_b, \tag{69}$$

where δ_a and δ_b are parameters characterizing the penetration depth. A similar condition has been used previously in a slightly different context by Moss et al. (1990a). For an oscillatory field $\delta = \delta_a = \delta_b = (T_{\rm cyc}\eta/\pi)^{1/2}$ is the skin depth, where η is the magnetic diffusivity of the interior. Assuming $\eta = 10^{-4}$ (in units of η_t) and $T_{\rm cyc} = 0.1$ we have $\delta = 0.002$. In the following, however, we consider δ_a and δ_b as free parameters.

Using Eq. (69) we now find oscillatory dynamo solutions for Model A− with dynamo waves migrating equatorwards. These two properties are rather insensitive to the exact values chosen for δ_a and δ_b. We also find similar oscillations using the boundary condition $a = b = 0$ at the lower boundary, ie $\delta_a, \delta_b \to 0$. In the following we present results for $\delta_a = \delta_b = 0.05$ (Run B1) and 0.002 (Run B2). A typical snapshot of the magnetic field and flow structure is shown in Fig. 11. Note that the gross structure of the field is qualitatively not very different from the oscillatory case for Model A+ using the perfect conductor boundary condition (Run T7). In contrast, with a perfect conductor boundary condition for Model A− we find steady solutions with field geometry that is quite different. This shows that the question whether or not the dynamo is oscillatory crucially depends on the treatment of the lower boundary condition, and that the field structure itself is less sensitive to such details once the solution is oscillatory.

The direction of magnetic field migration of Models A+ and A− for $C_\alpha > 0$ is different and it is therefore interesting to see, whether this has any effect on the phase relation of magnetic and thermal energies and luminosity; see Fig. 12. It turns out that δU and δE_M are now in antiphase, without delay as in the previous case. Luminosity maxima occur still shortly after magnetic maxima, indicating that this feature is robust to details of the model. Furthermore, δL is about ten times larger than in Run T7, ie $\delta L/L \approx 10^{-5}$.

© European Southern Observatory • Provided by the NASA Astrophysics Data System

1992A&A...265..328B

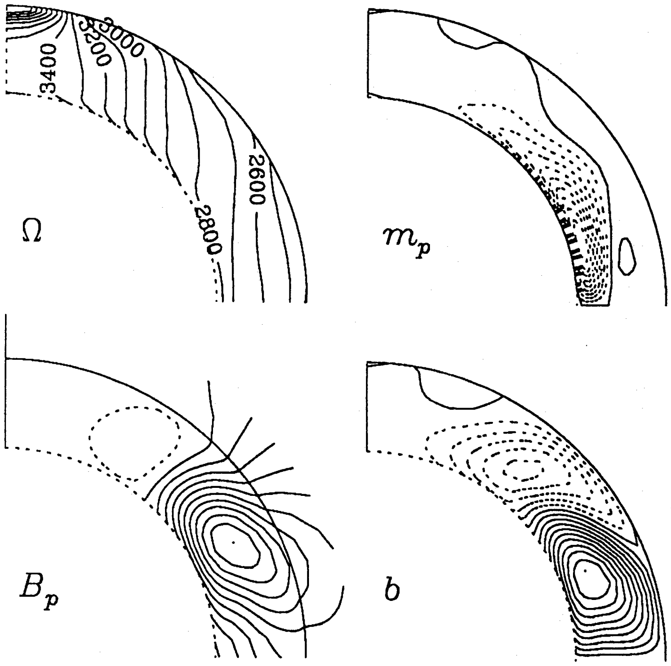

Fig. 11. Contours of angular velocity, streamlines of meridional mass flow, poloidal magnetic field lines, and contours of toroidal field, for Model A− for $C_\alpha = 10$ with the modified boundary condition for the magnetic field (Run B1)

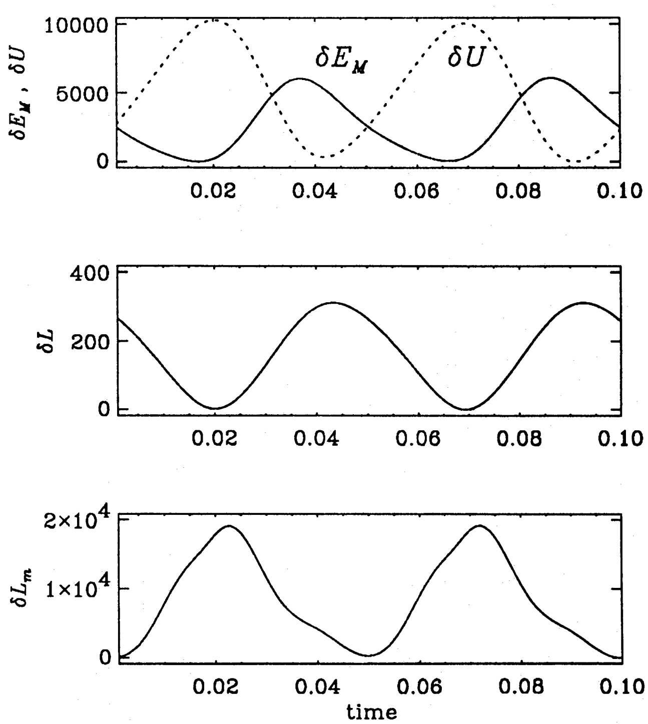

Fig. 12. Variation of magnetic and thermal energies (upper panel), and luminosity at the surface (second panel) and in the middle of the shell (third panel) for Model A− for $C_\alpha = 10$ with the modified boundary condition for the magnetic field (Run B1)

6. Remarks on the input quantities

There are a number of input parameters whose values are not exactly known, so it is important to discuss the sensitivity of our results to changes in such quantities.

The Λ-effect parameters are constrained to some extent by observations, e.g. Ω is smaller at the poles than at the equator and the rotation at the bottom of the convection zone is nearly rigid, being there close to the surface value at 30° latitude. If the Taylor number is below ca. 10^5 the Ω-contours are only weakly affected by the meridional flow and their shape then corresponds to that obtained in the approximation of neglecting meridional flows (see Fig. 2 in Kichatinov 1987). Observations suggest Λ-effect parameters similar to those used in Model B with lower Taylor numbers; see Fig. 2. For larger Taylor numbers the Ω-contours become more and more cylindrical. This Taylor-Proudman effect occurs almost independently of the details of the mechanism generating differential rotation. This conclusion is valid even in the presence of strong density stratification and convective energy transport. Thus, unless the effects of anisotropic heat transfer are really important, we have to conclude that Ta should be much less than $3\,10^7$.

In order to obtain dynamo action we have to choose the value of C_α large enough. In addition, in order that oscillatory dynamo solutions of $\alpha\Omega$-type are possible, $|C_\Omega|$ has to be large, which implies that the product $\mathrm{Pr}_M^2\mathrm{Ta}$ has to be large. Thus, if Ta is chosen to be small (see previous paragraph) then a large value of $|C_\Omega|$ can only be achieved with a large value of Pr_M (see Papers I, III). Increasing the value of $|V^{(0)}|$ also produces larger values of $|C_\Omega|$, but then the relative latitudinal variation of Ω becomes unrealistically large (see Paper II). Moreover, in one particular case we found that with an enhanced value of $|V^{(0)}|$ the dynamo is still not yet oscillatory (see Run L1 with $V^{(0)} = -1.5$), even though $|C_\Omega|$ is quite large. Oscillatory solutions with poleward migration (ie $\alpha\partial\Omega/\partial r > 0$) are possible for smaller values of $|C_\Omega|$ (cf. T5, T8 and I3, I4 in Table 2). The question of oscillatory solutions strongly depends on the lower boundary condition for the magnetic field and seems to be independent of stratification.

The ratio Ta/Γ determines the strength of baroclinic flows and the pole-equator variation of density and pressure. This ratio is well known for the Sun, but the resulting flows in the nonadiabatic case are much smaller than the flows generated by nonuniform rotation and magnetic fields; see Table 2.

The strength of stratification should be as large as possible in order to cover more of the regions close to the upper surface. However, increasing the degree of stratification further beyond the values adopted leads to changes primarily in the uppermost layers and plausibly has no important effects on the nature of the dynamo that operates in deeper layers; see Fig. 4.

The parameters $\mathscr{L}$ and Pr are crucial for the onset of large scale convection. The main uncertainty here comes from the adopted equation itself; see Eq. (9). The concept of describing turbulent convective energy transport as entropy diffusion, in particular, is too simple, if the assumption of a constant value for the eddy heat conductivity is made. A more detailed analysis might, however, lead to an automatic reduction of the transport efficiency, so that our artifice of taking $\mathscr{L}$ to be subcritical may not be too artificial.

Apart from the uncertainties in the α and Λ coefficients, the various diffusion coefficients are obviously ill-determined. Indeed, the whole concept of turbulent diffusivity may be inadequate to describe convective turbulence. For example, anisotropies and

© European Southern Observatory • Provided by the NASA Astrophysics Data System

1992A&A...265..328B

nonlocal effects may be important. Such issues hopefully can be addressed in the future by using high resolution direct simulations of turbulent hydromagnetic convection of the solar convection zone.

Finally, we should note that the neglect of turbulent viscous heating in Eq. (3) may not actually be justified. In general, the turbulent viscous heating source term is given by $q_{\rm visc} = -u_{i,j}Q_{ij}$. The largest contribution comes from the differential rotation, ie $q_{\rm visc} \approx \rho\nu_t(\varpi\nabla\Omega)^2$. The integral of this term over the convection zone can be of the order of 10% of the solar luminosity.

7. Conclusions

The main purpose of the present paper is to describe the method and first results for mean-field models of dynamo action and differential rotation, including the effects of stratification and convective energy transport. It turns out that the stratified and unstratified cases are qualitatively similar in many respects. For example, the radial profiles of magnetic and kinetic energy densities, have similar shapes in the two cases (Fig. 4). The total magnetic and kinetic energies are also similar, but in the stratified case more magnetic energy goes into the poloidal field and the Ω-effect is quenched more significantly (Table 2). Including nonadiabaticity and energy transport has either only secondary effects (luminosity variations etc) or, if the turbulent Rayleigh number exceeds a critical value, the solution is strongly governed by large scale convection which, however, may be an artefact of the model; see Sect. 5.3. If we adopt solar values for luminosity, gravity and rotation then we can only obtain subcritical values for the turbulent Rayleigh number if the Prandtl number is reduced to ca. 0.1. For such models the mean meridional flow is ca. 8-20 m/s in the absence of magnetic fields, but varies between 20 and 80 m/s if a cyclic magnetic field is present. At the bottom of the convection zone this field can reach values of the order of 6 kgauss which is about the equipartition value. Furthermore, cycle variations in the luminosity are quite small, even though the thermal energy varies substantially with the magnetic cycle.

A somewhat surprising result is that cylindrical Ω-contours occur – see Figs. 1, 3, 7, and 12 – even in the presence of strong stratification, at least near the equator. Thus, the Taylor-Proudman theorem, which applies in the incompressible case in the limit of vanishing viscosity, seems to hold approximately also in the compressible case with stratification and in the presence of relatively strong magnetic fields. Deviations can occur close to the surface or be caused by a strongly anisotropic heat conductivity tensor. The latter possibility implies that the latitudinal convective flux exceeds significantly the vertical convective flux (see Fig. 10) which may be hard to justify (Durney 1976).

We have only considered flows and dynamo action in the bulk of the convection zone, ie the interaction between the convection zone and the stably stratified interior beneath has been neglected. This interaction may well be important and clearly needs to be investigated further. In certain circumstances, this may be equivalent to saying our results are sensitive to the treatment of the lower boundary condition. There is further evidence for this in that whether or not the solutions are oscillatory crucially depends on the lower boundary condition for the magnetic field. The perfect conductor boundary condition may be inadequate, because magnetic fields penetrate to some extent into the interior. Experiments show that other lower boundary conditions can readily produce oscillatory solutions; see Sect. 5.8. This illustrates the importance of including at least part of the interior in the model in a consistent manner. A practical difficulty is that the value of the effective diffusivity decreases very rapidly below the overshoot layer from its value at the bottom of the convection zone, which causes numerical difficulties for models extending into this region. Results with a smaller value of the magnetic diffusivity in the interior can be found in Roberts & Stix (1972) for the kinematic case and in Paper III for the nonlinear case with Λ effect.

There are a number of further problems in explaining the solar magnetic activity cycle in terms of "distributed" mean-field dynamo theory. One of these is related to the effects of magnetic buoyancy removing flux from the convection zone on a time scale shorter than the cycle period. (However, following the simulations of Nordlund et al. (1992), it may be that these difficulties attributed to distributed dynamos have been overstated.) For these reasons, the dynamo has thus often been placed in a rather *ad hoc* manner at the bottom of the convection zone. A number of such models have been designed with negative α effect and positive $\partial\Omega/\partial r$ at the equator. This ensures equatorward migration of the activity belts, but produces the wrong phase relation between poloidal and toroidal fields. These and many other models rely on assumed distributions of α effect and differential rotation. However, it is important to remember that the migration properties can be strongly affected by turbulent pumping mechanisms (Kichatinov 1991). For example, in the presence of a strong turbulent downward transport, dynamo waves can migrate equatorwards even though $\alpha\partial\Omega/\partial r > 0$ (Paper III).

Another common feature of many αΩ-type dynamos is that the cycle period is one order of magnitude shorter than the solar 22 year magnetic cycle period. It is interesting to note that the period in the compressible convective dynamo models of Glatzmaier (1985) is much longer (about 10 yr) than in the incompressible models of Gilman (1983), who found periods of about 1.5 yr. In our models the period is also short (1 - 3 yr), but only for Model B there is a significant increase of the period in the compressible as compared to the incompressible case.

Our formalism represents an alternative route forward that is a compromise between the computationally expensive larger scale global simulations pioneered by Gilman and Glatzmaier, and the grossly over-simplified kinematic or quasi-kinematic models. In the three-dimensional globally consistent models by Gilman (1983) and Glatzmaier (1985) the hydromagnetic equations are solved, and magnetic fields and differential rotation occur as a consequence of large scale convection. In contrast to α-effect models, there is no dynamo effect from the small scale motions. These models typically lead to a *poleward* migration of magnetic activity belts as do most of our models (Runs T7, T9, N2, N3, I2, I3). We represent the effects of the small scale motions on both the angular momentum transport and the magnetic field, whilst retaining the essential physics of the convection zone. Computational times are then short enough to allow adequate exploration of parameter space. An obvious problem with our formalism is that we need to know values and functional forms of the various turbulence parameters that enter our equations. In principle, these values are related, and are indeed known given a suitable turbulence model. In practice, at the moment they are to an extent arbitrary and independent of one another. In the reasonably near future it may be possible to derive self-consistent expressions for these coefficients from numerical simulations of compressible hydromagnetic convection (e.g. Brandenburg et al. 1990b; Pulkkinen et al. 1991), which will, in principle, reduce the number of degrees of freedom present.

© European Southern Observatory • Provided by the NASA Astrophysics Data System

1992A&A...265..328B

Acknowledgements. The computations were performed on the Convex 220 and the Cray X-MP/432 of the Centre for Scientific Computing, Espoo, Finland.

References

Brandenburg, A., Krause, F., Meinel, R., Moss, D., Tuominen, I.: 1989, *Astron. Astrophys.* **213**, 411
Brandenburg, A., Moss, D., Rüdiger G., Tuominen, I.: 1990a, *Solar Phys.* **128**, 243 (Paper I)
Brandenburg, A., Nordlund, Å., Pulkkinen, P., Stein, R.F., Tuominen, I.: 1990b, *Astron. Astrophys.* **232**, 277
Brandenburg, A., Moss, D., Rüdiger G., Tuominen, I.: 1991a, *Geophys. Astrophys. Fluid Dyn.* **61**, 179 (Paper II)
Brandenburg, A., Moss, D., Rieutord, M., Rüdiger G., Tuominen, I.: 1991b, In *The Sun and cool stars: activity, magnetism, dynamos* (ed. I. Tuominen, D. Moss & G. Rüdiger), Lecture Notes in Physics **380**, Springer-Verlag p.147
Brandenburg, A., Moss, D., Tuominen, I.: 1992, in *The Solar Cycle*, ed. K. L. Harvey, Astron. Soc. Pacific Conf. Proc., in press (Paper III)
Brown, T. M., Morrow, C. A.: 1987, *Astrophys. J.* **314**, L21
Chandrasekhar, S.: 1961, *Hydrodynamic and Hydromagnetic Stability.* Oxford, Clarendon Press
Durney, B. R.: 1976, *Astrophys. J.* **204**, 589
Durney, B. R., Roxburgh, I. W.: 1971, *Solar Phys.* **16**, 3
Gilman, P. A.: 1983, *Astrophys. J. Suppl.* **53**, 243
Gilman, P. A., Miller, J.: 1981, *Astrophys. J. Suppl.* **46**, 211
Glatzmaier, G. A., Gilman, P. A.: 1981, *Astrophys. J. Suppl.* **45**, 351
Glatzmaier, G. A., Gilman, P. A.: 1982, *Astrophys. J.* **256**, 316
Glatzmaier, G. A.: 1985, *Astrophys. J.* **291**, 300
Gough, D.: 1969, *J. Atmos. Sci.* **26**, 448
Ivanova, T. S., Ruzmaikin, A. A.: 1977, *Sov. Astron.* **21**, 479
Jennings, R. L.: 1991, *Geophys. Astrophys. Fluid Dyn.* **57**, 147
Jennings, R., Brandenburg, A., Moss, D., Tuominen, I.: 1990, *Astron. Astrophys.* **230**, 463
Jepps, S. A.: 1975, *J. Fluid Mech.* **67**, 625
Köhler, H.: 1970, *Solar Phys.* **13**, 3
Kichatinov, L. L.: 1987, *Geophys. Astrophys. Fluid Dyn.* **38**, 273
Kichatinov, L. L.: 1991, *Astron. Astrophys.* **243**, 483
Libbrecht, K.G.: 1988, in E. J. Rolfe (ed.), 'Seismology of the Sun and Sun-like Stars', ESA SP-286, 131
Moss, D. L., Mestel, L., Tayler, R. J.: 1990a, *Monthly Notices Roy. Astron. Soc.* **245**, 550
Moss, D., Tuominen, I., Brandenburg, A.: 1990b, *Astron. Astrophys.* **240**, 142
Nordlund, Å., Brandenburg, A., Jennings, R. L., Rieutord, M., Ruokolainen, J., Stein, R. F., Tuominen, I.: 1992, *Astrophys. J.* **392, 647**
Parker, E. N.: 1987, *Astrophys. J.* **321**, 984
Pulkkinen, P., Tuominen, I., Brandenburg, A., Nordlund, Å., Stein, R.F.: 1991, In *The Sun and cool stars: activity, magnetism, dynamos* (ed. I. Tuominen, D. Moss & G. Rüdiger), Lecture Notes in Physics **380**, Springer-Verlag p.98
Roberts, P. H., Soward, A. M.: 1975, *Astron. Nachr.* **296**, 49
Roberts, P. H., Stix, M.: 1972, *Astron. Astrophys.* **18**, 453
Rüdiger, G.: 1973, *Astron. Nachr.* **294**, 183
Rüdiger, G.: 1980, *Geophys. Astrophys. Fluid Dyn.* **16**, 239
Rüdiger, G.: 1989, *Differential rotation and Stellar Convection: Sun and solar-type stars*, Gordon & Breach, New York
Rüdiger, G., Tuominen, I.: 1987, In *The Internal Solar Angular Velocity* (ed. B. R. Durney & S. Sofia), D. Reidel, Dordrecht p.361
Rüdiger, G., Tuominen, I.: 1990, In *Solar Photosphere: Structure, Convection and Magnetic Fields* (ed. J. O. Stenflo), Kluwer Acad. Publ., Dordrecht p.315
Rüdiger, G., Kichatinov, L. L.: 1990, *Astron. Astrophys.* **236**, 503
Rüdiger, G., Tuominen, I., Krause, F., Virtanen, H.: 1986, *Astron. Astrophys.* **166**, 306
Schmidt, W.: 1982, *Geophys. Astrophys. Fluid Dyn.* **21**, 27
Schmitt, D., Schüssler, M.: 1989, *Astron. Astrophys.* **223**, 343
Schüssler, M.: 1979, *Astron. Astrophys.* **72**, 348
Schwarzschild, M.: 1958, *Structure and evolution of the stars*, Princeton University Press, New Jersey
Spiegel, E. A., Weiss, N. O.: 1980, *Nature* **287**, 616
Spruit, H. C.: 1977, *Astron. Astrophys.* **55**, 151
Stix, M.: 1989, *Rev. Mod. Astron.* **2**, 248
Tuominen, I., Rüdiger, G.: 1989, *Astron. Astrophys.* **217**, 217
Vainshtein, S., Levy, E. H.: 1991, *Solar Phys.* **135**, 261
Weiss, N. O.: 1965, *Observatory* **85**, 37

This article was processed by the author using Springer-Verlag LaTeX A&A style file 1990.

© European Southern Observatory • Provided by the NASA Astrophysics Data System